LIGO Laboratory / LIGO Scientific Collaboration

LIGO-T0900334-v2 *ADVANCED LIGO* 7/8/09

Response to:
Stray Light Control PDD Comments

Michael Smith, Riccardo DeSalvo, Niem Nguyen, Mohana Mageswaran, Ken Mailand, Virginio Sannibale, Phil Willems, Luke Williams

Distribution of this document:
LIGO Science Collaboration

This is an internal working note
of the LIGO Project.

California Institute of Technology
LIGO Project – MS 18-34
1200 E. California Blvd.
Pasadena, CA 91125
Phone (626) 395-2129
Fax (626) 304-9834
E-mail: info@ligo.caltech.edu

Massachusetts Institute of Technology
LIGO Project – NW22-295
185 Albany St
Cambridge, MA 02139
Phone (617) 253-4824
Fax (617) 253-7014
E-mail: info@ligo.mit.edu

LIGO Hanford Observatory
P.O. Box 1970
Mail Stop S9-02
Richland, WA 99352
Phone 509-372-8106
Fax 509-372-8137

LIGO Livingston Observatory
P.O. Box 940
Livingston, LA 70754
Phone 225-686-3100
Fax 225-686-7189

http://www.ligo.caltech.edu/

Table of Contents

Table of Tables

Table of Figures

Abstract

This document responds to the questions posed by the SLC PDR committee.

1 Introduction

1.1 Purpose

This document responds to the questions posed by the SLC PDR committee.

1.2 Applicable Documents

1.2.1 LIGO Documents

T0900312-v1, Reference Seismic Data for LLO

T0900285-v1, L1 HAM6 ISI eLIGO Final Performance Measurements (June 5, 2009)

T000083-01, COS Faraday Isolator Pre-alignment Procedure

T0900269-v2, AOS SLC PDD

T0900324-v1, Design Equations for Initially Flat Blade Springs at Arbitrary Mounting Angles

2 List of Issues to be Addressed

2.1 LLO BSC Wall Motion

2.1.1.1 Seismic Motion of the Vacuum Manifold

The seismic motion of the LLO LVEA vacuum beam line (90% probability data) is compared with the seismic motion at LHO, which was used to calculate the scattered light, as shown in Figure 1. See T0900312-v1, Reference Seismic Data for LLO

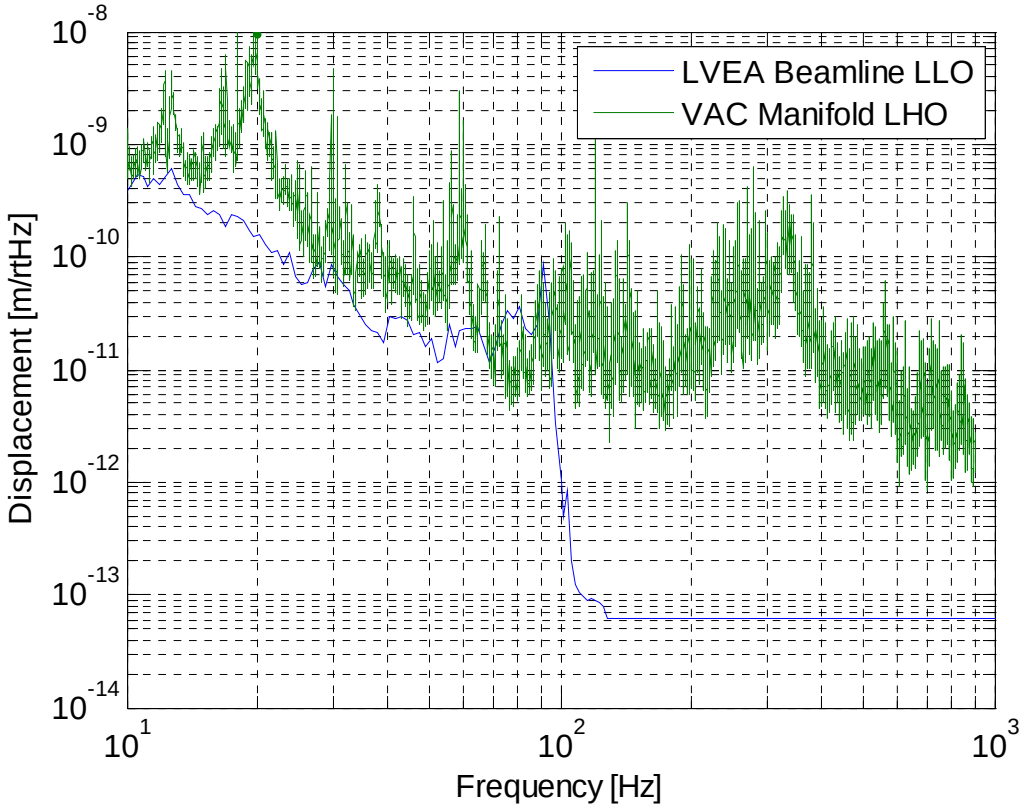

Figure 1: Seismic motion of vacuum manifold

The following scattered light sources depend upon the vacuum manifold motion, and would actually be less at LLO:

`Signal_AC_Baffle_Refl,`

`Signal_Total_BSC_Manifold_Wide_Angle,`

`Signal_Cryo_Baffle_Power,`

`Signal_Cryo_Baffle_Refl_Power,`

`Signal_ITM_GBHR3_ARMBAF_Power,`

`Signal_ITM_GBHR4_ARMBAF_Power,`

```
Signal_BS_GBAR3X_ARMBAF_Power
Signal_BS_GBAR4X_ARMBAF_Power,
Signal_BS_GBHR3X_ARMBAF_Power,
Signal_BS_GBHR4X_ARMBAF_Power,
Signal_PR3_GBHR_Total,
Signal_SR3_GBHR_Total
```

2.2 Noise Assessments for Expected LLO BSC HEPI Motion

A comparison of the ISI "0" (HEPI) motion and the Brian Lantz SEI elog entry ID: 596, 3/14/06, is shown in **Figure 2**.

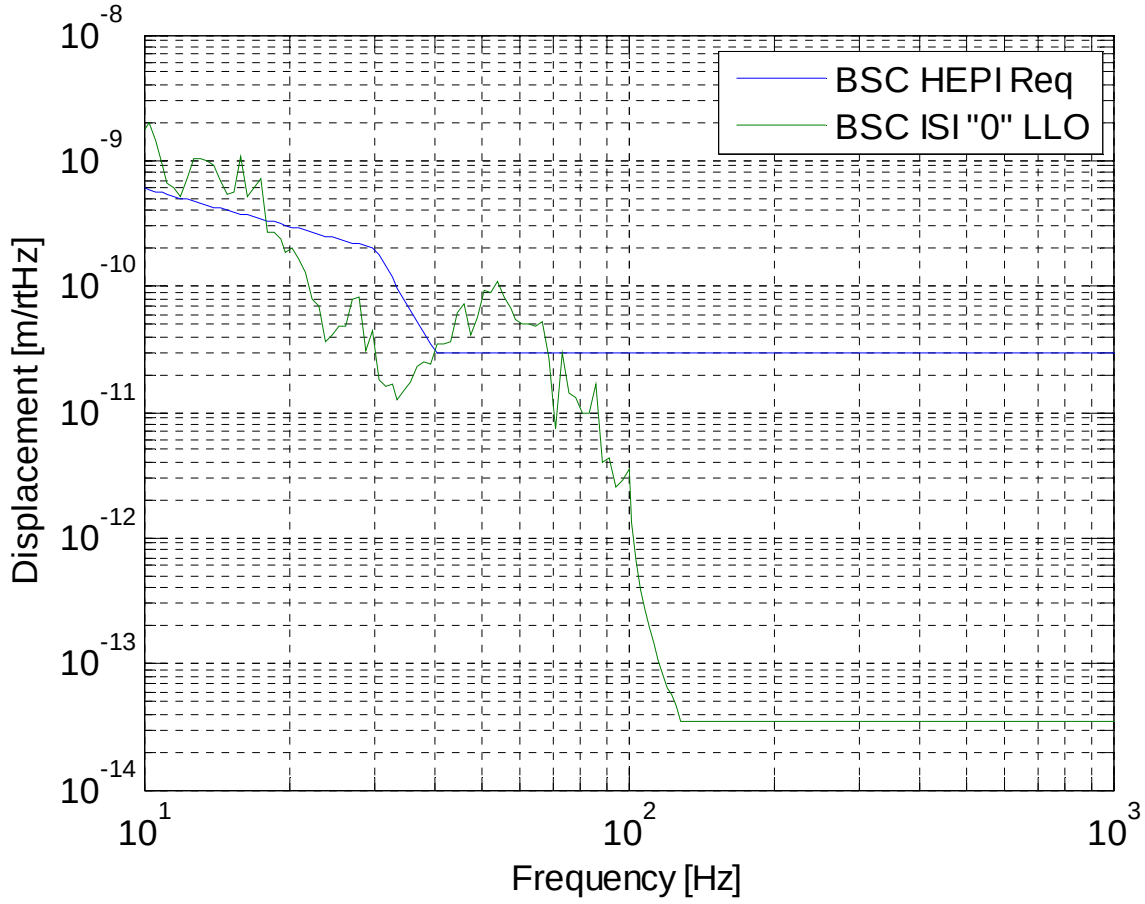

Figure 2: BSC ISI "0" Motion Spectrum

The Arm Cavity Baffle, the COC Wide Angle Baffle, and the Elliptical Baffle are all suspended from the BSC ISI "0" ring. The scattering was recalculated using the measured LLO BSC ISI "0" ring motion.

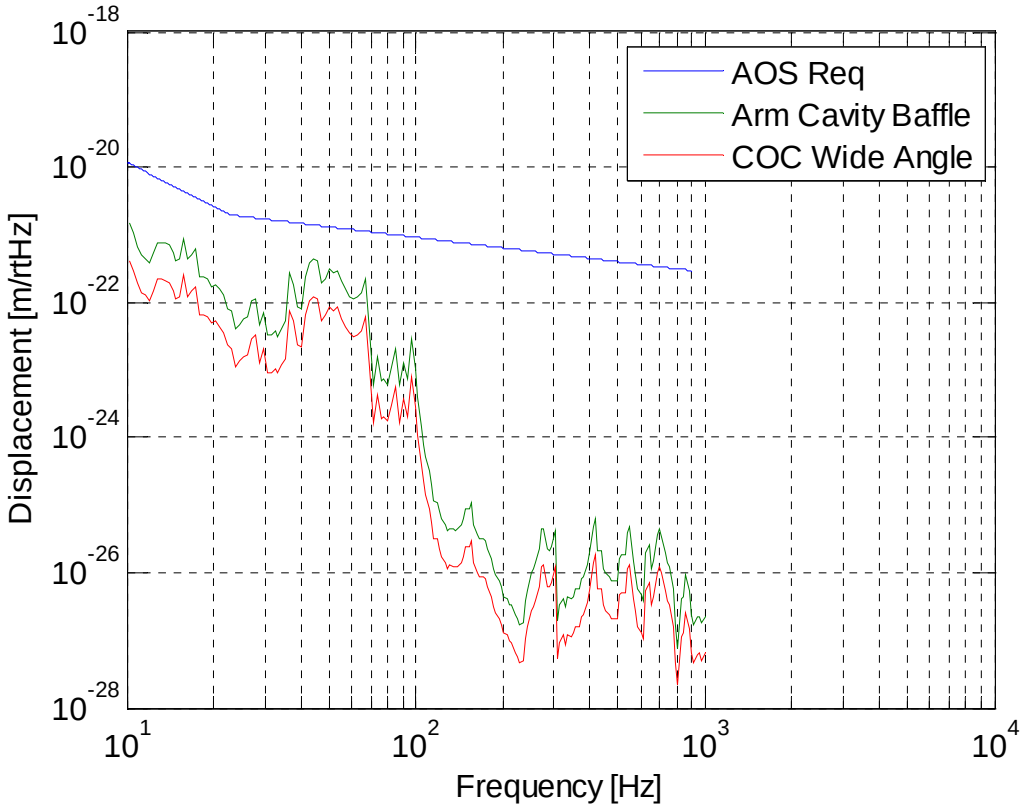
AOS Req
Arm Cavity Baffle
COC Wide Angle
Displacement [m/rtHz]
Frequency [Hz]
10^-18
10^-20
10^-22
10^-24
10^-26
10^-28
10^1
10^2
10^3
10^4

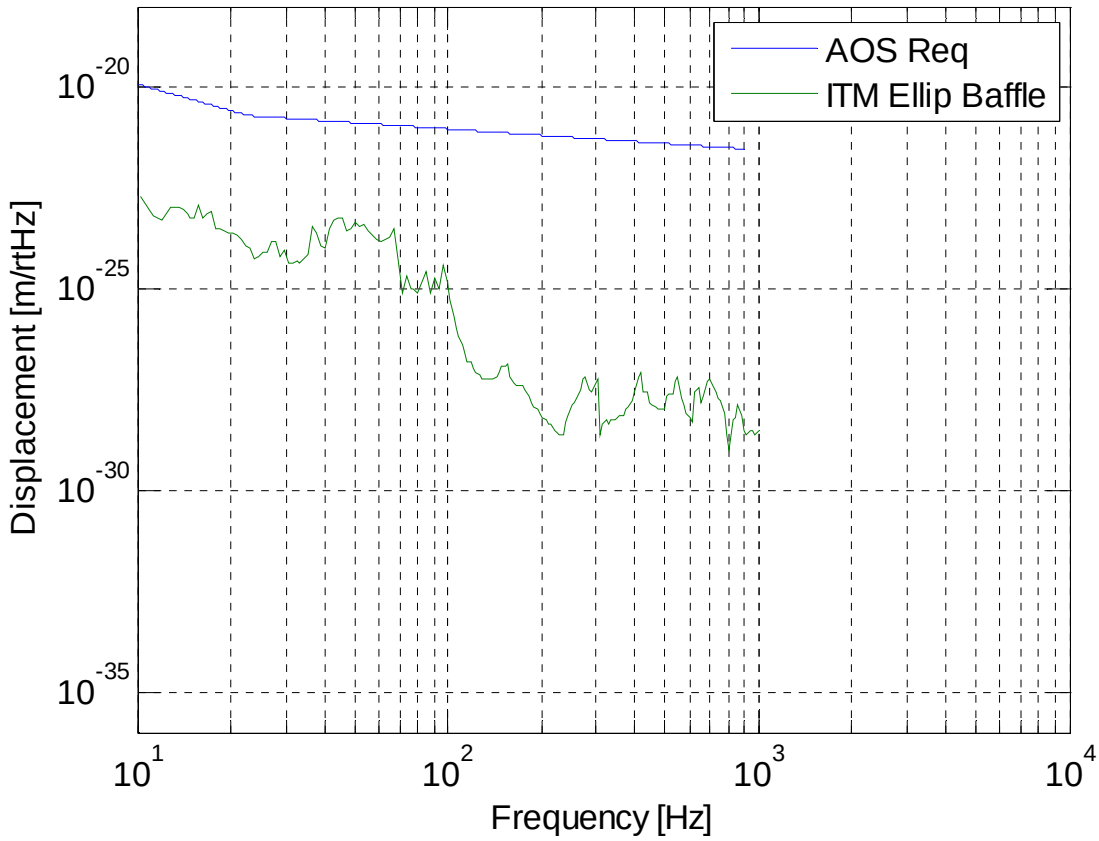

2.3 Need for Better Baffle Material?

The scattered light displacement noise from all oxidized SS baffles and beam dumps is shown in Figure 3. The BRDF of oxidized SS gives an adequate margin for all of the surfaces.

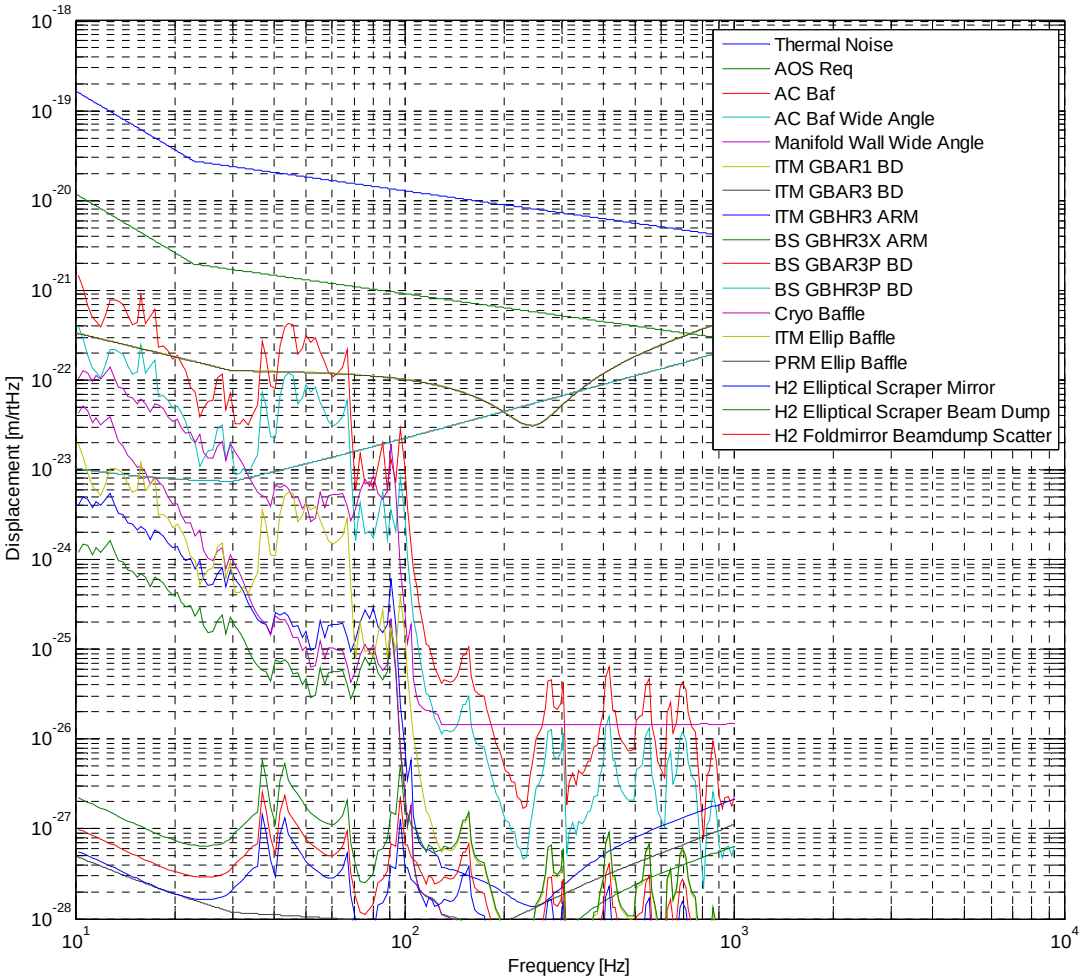

Figure 3: Scattered Light Noise from all Oxidized SS Baffle Surfaces

2.4 Scraper Baffles and Plate Dumps

The purpose of the PR2 and SR2 scraper baffles is to catch the ghost beams produced by the BS, ITM, and CP. In addition, these scraper baffles catch the HR side ghost beams from the PR2 and SR2 mirrors.

2.4.1 PR2 Scraper Baffle

A model of the PR2 baffle is shown in Figure 4. The horizontal aperture of the PR2 scraper baffle allows a >6.2 mm clearance from the edges of the power recycling cavity beams in the vicinity of PR2, as shown in Figure 5.

The BS and CP ghost beams are also dumped on the baffle.

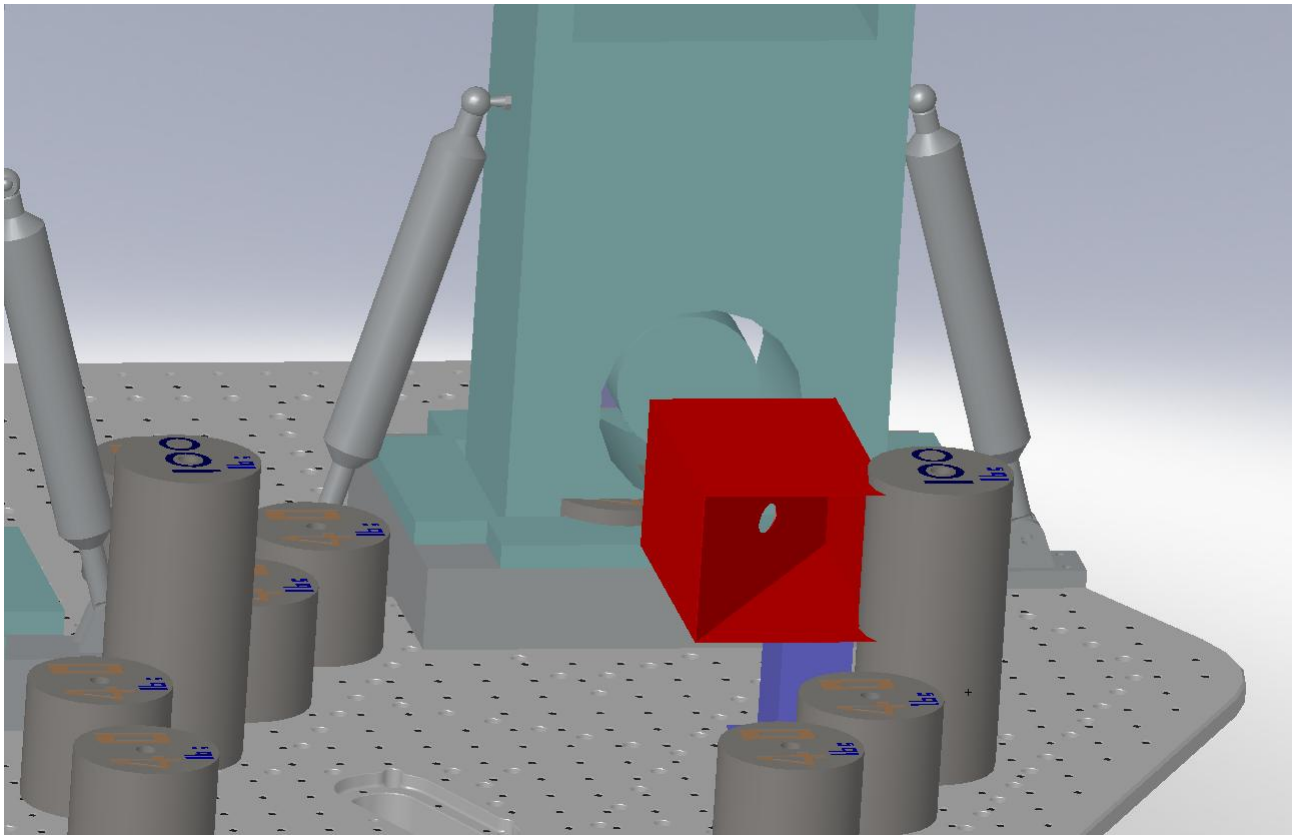

Figure 4: PR2 Model on HAM3

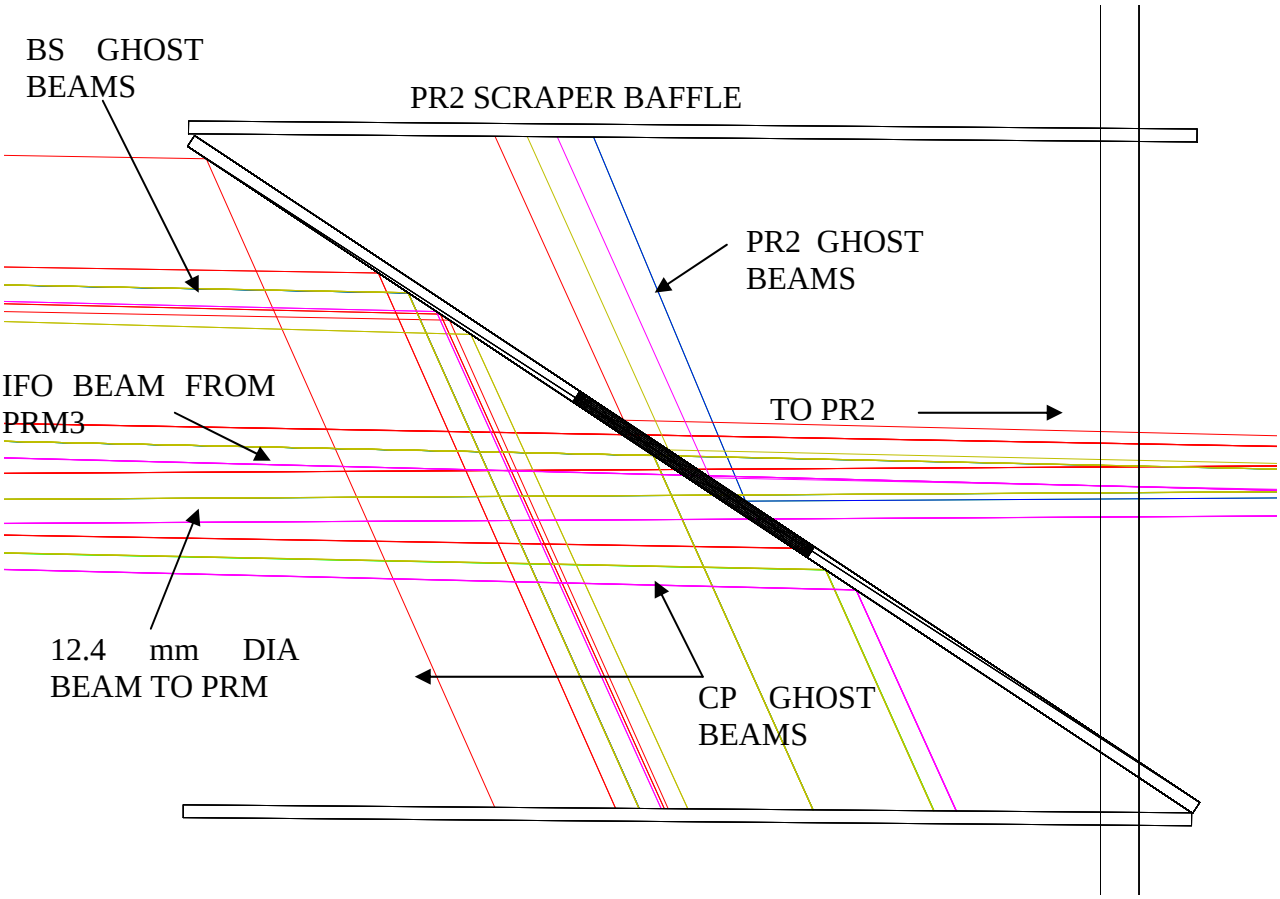

Figure 5: PR2 Scraper Baffle, top view

The aperture in the vertical direction provides a 6.2 mm clearance from the edges of the power recycling cavity beams shown in Figure 6.

The PR2 GBHR, CP, and ITM GBAR ghost beams are also dumped on the baffle.

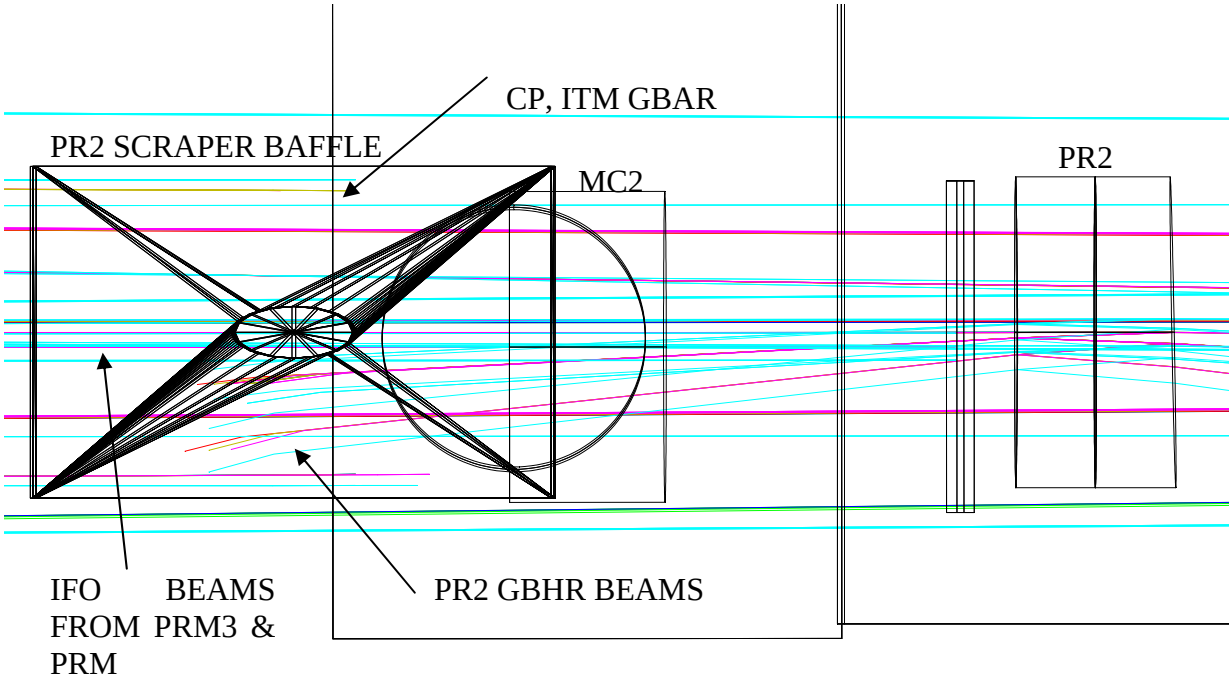

Figure 6: PR2 Scraper Baffle, side view

2.4.2 SR2 Scraper Baffle

The horizontal aperture of the SR2 scraper baffle allows a >8.2 mm clearance from the edges of the power recycling cavity beams in the vicinity of SR2, shown in Figure 7.

The BS and CP ghost beams are also dumped on the baffle.

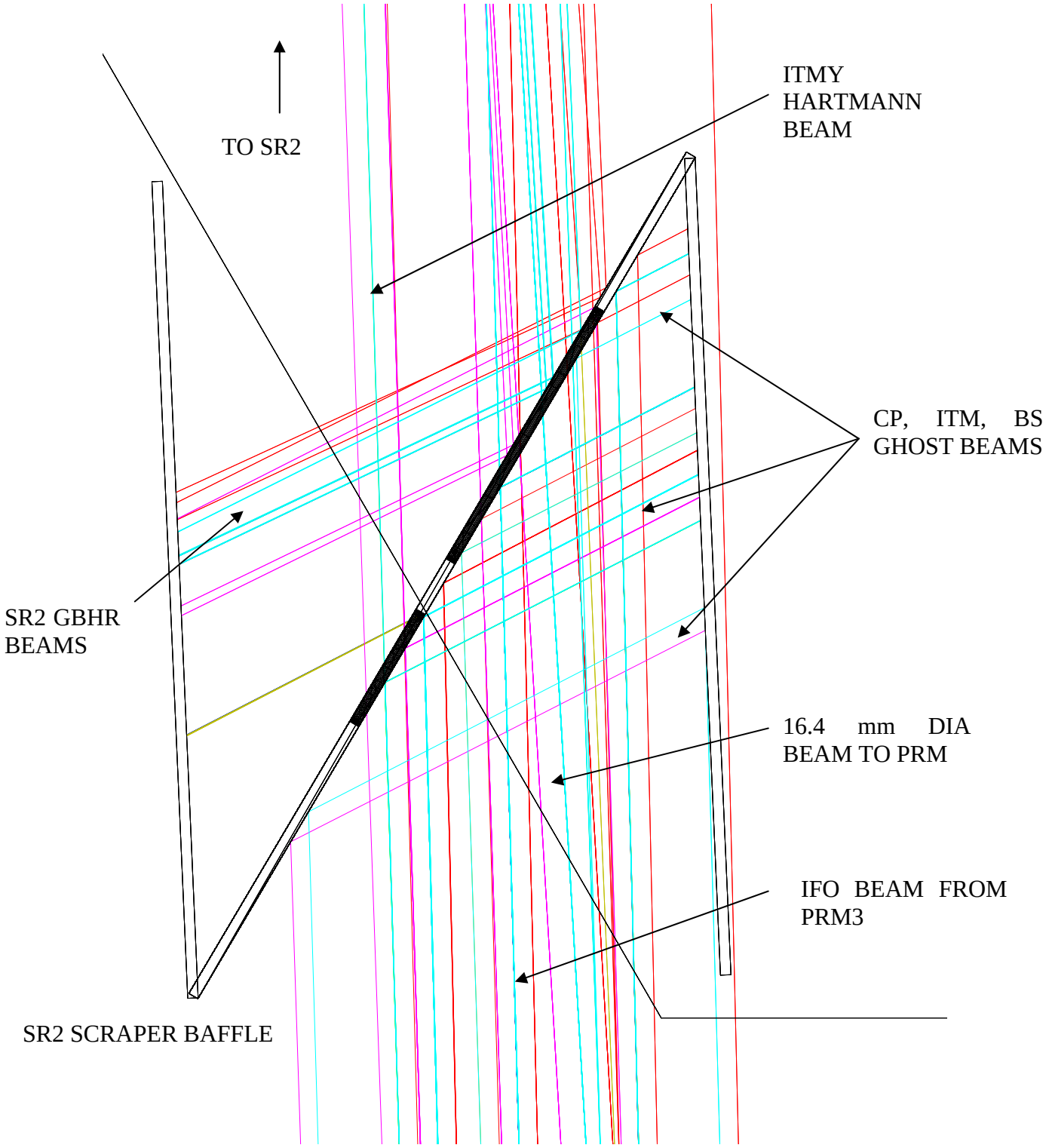

Figure 7: SR2 Scraper Baffle, top view

The aperture in the vertical direction provides a >8.2 mm clearance from the edges of the power recycling cavity beams shown in Figure 6.

2.4.3 Mass Budgets for Baffles and Beam Dumps

Table 1: Mass Budgets for Baffles and Beam Dumps

Name	**Location**	**Mass**
Output Faraday Isolator	HAM5, HAM11	
Arm Cavity Baffle & Wide angle	BSC1, BSC3, BSC7, BSC8	195
Wide Angle Baffle	BSC1, BSC3, BSC7, BSC8	65
ITM Elliptical Baffle	BSC2, BSC4	100
FM Elliptical Baffle	BSC7, BSC8	21
FM Beam Dump	BSC7, BSC8	33
Manifold/Cryopump Baffle	ITM Manifold	380 lbs
PR2 and SR2 Scraper Beam Dumps	HAM3, HAM4, HAM9, HAM10	15

2.4.4 Is Edge Diffraction and Scattering from Baffles Near a COC Important?

2.4.4.1 Edge Diffraction from Near-by Baffles

Diffraction from the edge of the Arm Cavity Baffle was calculated. The calculation is similar to the calculation for the Mid-station Baffle.

We will assume that the circumference of the baffle edge is unwrapped to form a linear edge. The circumference is 1.08 m.

The following parameters differ in the calculation: 1) the distance from the edge to the nearby TM is 0.5 m, compared to 2000 km; 2) the angle subtended by the edge at the center of the TM is 0.33 rad, compared to 30 E-6 rad; 3) the BRDF of the TM is 3.4E-7, compared to 1364—this appears to be a good deterrent against coupling into the IFO mode; 4) the incident power is 55W, instead of 22 W.

The diffracted light displacement noise @ 20 Hz is

$$DN_{aced} = 1.908\times 10^{-33}$$

Compared to

$$DN_{mbed} = 2.862\times 10^{-34}$$

Both values are remarkably similar, in spite of the different parameters used for the calculation.

Therefore, it appears that edge diffraction from nearby apertures is not important because the coupling into the IFO mode is small due to the small BRDF of the COC at large angles.

2.4.4.2 Wide-Angle Scattering from Near-by Baffles

The wide angle scattering from the H2 ITM HR hits the FM Scraper Mirror. The scattering from this source is calculated.

The wide-angle scattered power hitting the FM Scraper Mirror is, W

hemispherical scattering loss factor
ITM wide angle

$$\alpha_{ws} := 10. \times 10^{-6}$$

$$P_{fmsb} := P_a \cdot \int_{\theta_{fmsbi}}^{\theta_{fmsbo}} \frac{\alpha_{ws} \cdot \cos(\theta)}{\pi} \cdot 2 \cdot \pi \cdot \sin(\theta)\, d\theta$$

$$P_{fmsb} = 0.5132$$

Power scattered back into the IFO mode is, W

$$P_{fmsbackifo} := \sqrt{4} \cdot P_a \cdot \left(C_2 \cdot \alpha_{ws}^{2} \cdot \frac{\lambda^2}{L_{fmb}^{2}} \cdot BRDF_{H2scrmir} \right) \cdot T_{itmhu}$$

$$P_{fmsbackifo} = 2.2259 \times 10^{-22}$$

Displacement noise @ 20 Hz, m/rtHz

$$DN_{fmswaifo} := TF_{itmhr} \cdot \left(\frac{P_{fmsbackifo}}{P_{psl}} \right)^{0.5} \cdot x_{hepi} \cdot 2 \cdot k \cdot fmsatten$$

$$DN_{fmswaifo} = 4.9035 \times 10^{-23}$$

This is below the AOS requirement.

2.4.5 Do We Need PRM, SRM, PR2, SR2, PR3, SR3 Plate Beam Dumps?

The displacement noise from the PRM, PR2, and PR3 ghost beams, if they were allowed to hit the chamber walls, is several orders of magnitude below the AOS requirement, as seen in Figure 8.

The beam dumps for PR3, PR2, and PRM cause negligible displacement noise and will be eliminated.

The PRM plate beam dump will be retained as an errant beam baffle to protect the AR side of the PRM from an errant SM2 mirror. The errant beam baffle will be made of silicon carbide.

The beam dumps for SR3, SR2, and SRM will be maintained.

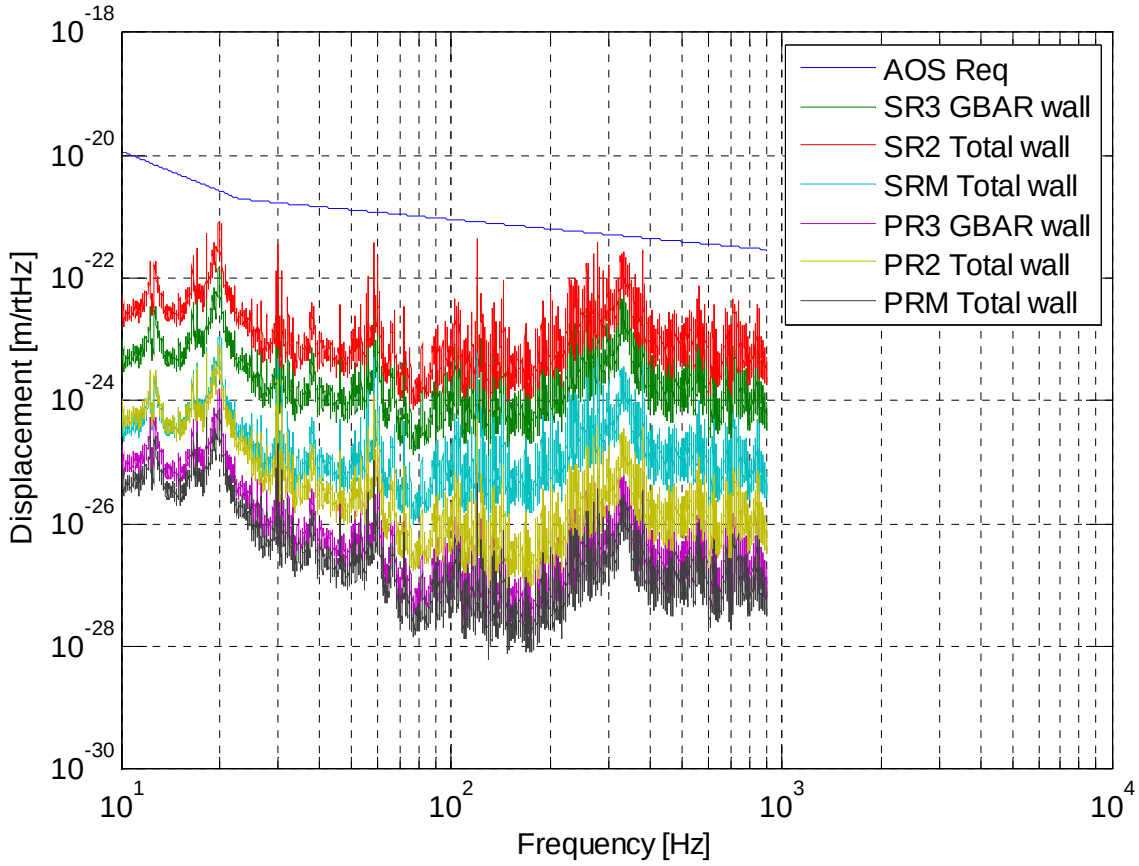

Figure 8: Displacement Noise of PR3, PR2, PRM, SR3, SR2, and SRM hitting the chamber walls.

2.4.5.1 SRM Plate Beam Dumps

The SRM internal ghost beams that exit the HR surface are caught with the SRM Output plate beam dump made from AR-coated black glass. The 25 mm diameter aperture of the plate beam dump provides a >10 mm clearance from the edges of the Signal Recycling beam.

Similarly, the internal ghost beams that exit the HR surface of the SRM are caught with the SRM Output plate beam dumps made from AR-coated black glass. The 25 mm diameter aperture of the plate beam dump provides a >10 mm clearance from the edges of the Signal Recycling beam.

2.4.5.2 PR2 and SR2 Plate Beam Dumps

The SR2 internal ghost beams that exit the AR surfaces are caught with the Output plate beam dumps made from AR-coated black glass. The aperture of the plate beam dump provides a >8.2 mm clearance from the edges of the Power Recycling and Signal Recycling beams.

The SR2 Input plate beam dump has been eliminated. Instead, the internal ghost beams that exit the HR surfaces of the SR2 are caught with the SR2 scraper baffles.

2.4.5.3 SR3 Plate Beam Dumps

The SR3 internal ghost beams that exit the AR surfaces are caught with the plate beam dump made from AR-coated black glass.

2.5 Output Faraday Isolator

2.5.1 HAM ISI data

The amplitude spectral densities for H1 HAM6 with the HAM ISI operating are presented in T0900285-v1. The x, y, and z degrees of freedom are shown in Figure 9.

The y-direction appears to be the worst case, and this data will be used for the scattered light calculations for surfaces mounted to the HAM optical tables.

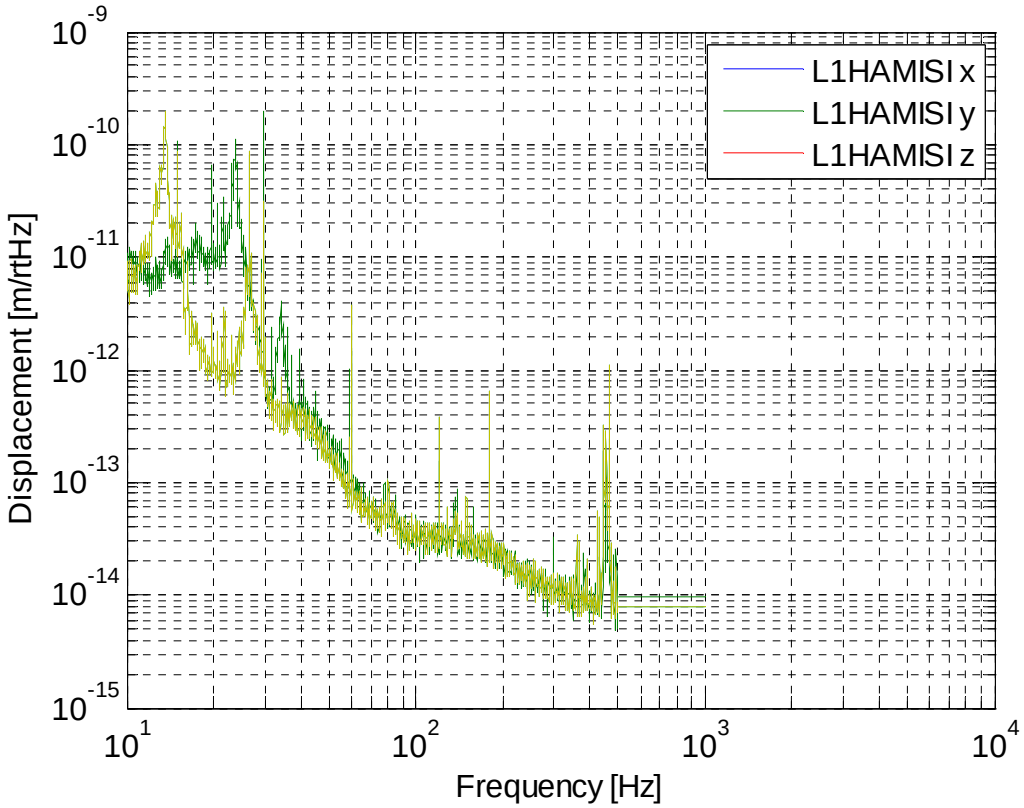

Figure 9: H1 HAM6 ISI data for x, y, and z degrees of freedom

2.5.2 Performance of Initial LIGO Output Faraday Isolator

The performance of the Initial LIGO Output Faraday Isolator was measured during the pre-alignment procedure at LHO (see T000083-01).

Transmissivity	98%
Power extinction ratio	4E-5

2.5.3 Eddy Current Damping Plate: Suspended or Attached to Frame?

The calculated horizontal motion transfer functions for the Output Faraday Isolator suspension are shown in Figure 10. The green curve corresponds to the eddy current damper being mounted directly to the suspension frame.

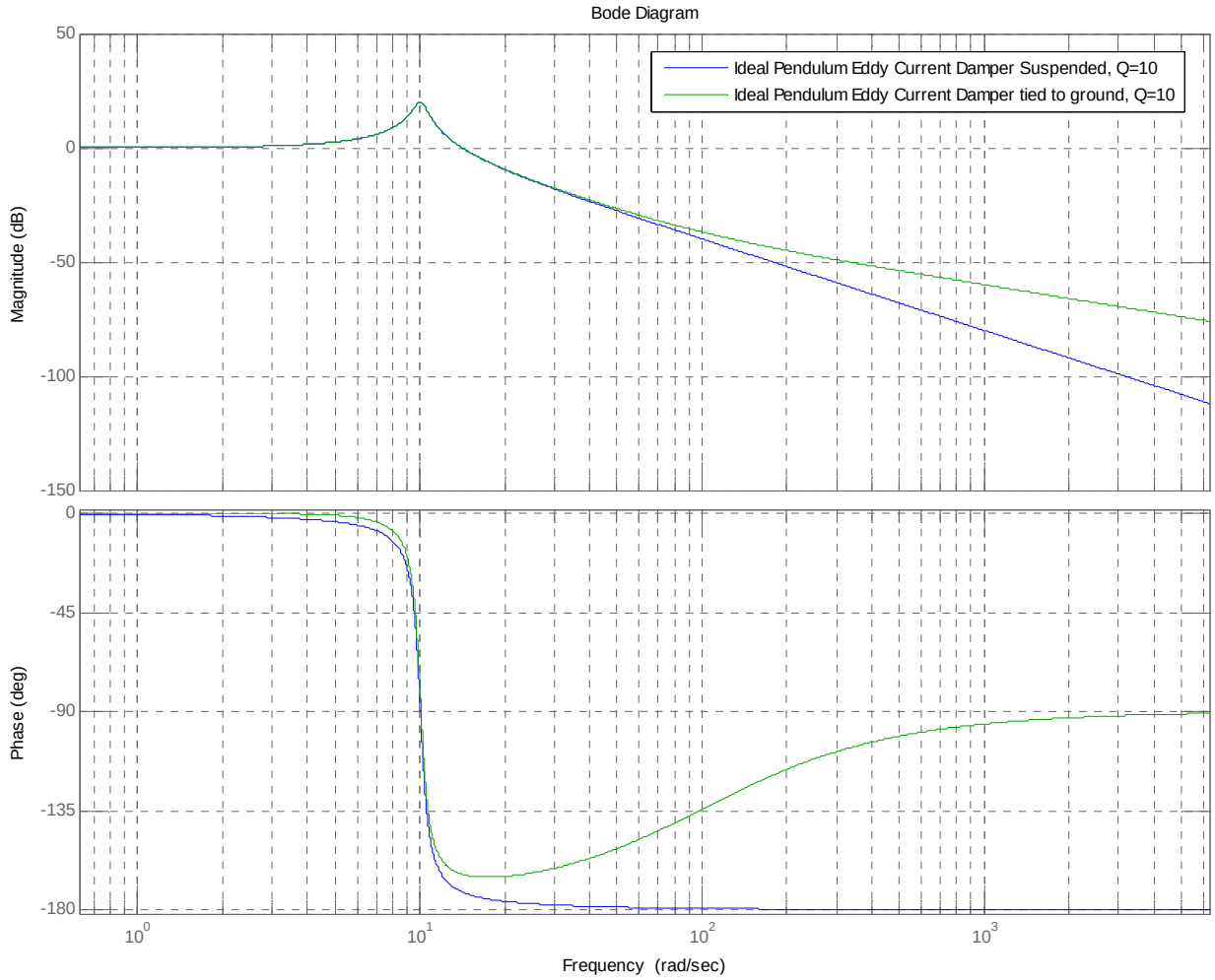

Figure 10: Transfer Functions for Eddy Current Damping: (blue curve) suspended damping plate, (green curve) eddy current damping plate mounted to frame

The scattered light displacement noise from the Input Faraday Isolator mounted to the HAM ISI platform is shown in Figure 11. Faraday Scatter1 is calculated with the eddy current damper attached to frame, and Faraday Scatter 0 is calculated with the eddy current damper suspended by a simple pendulum.

Therefore within the 10 – 1000 Hz range, the isolation is adequate if we attach the magnetic damping plate directly to the suspension frame.

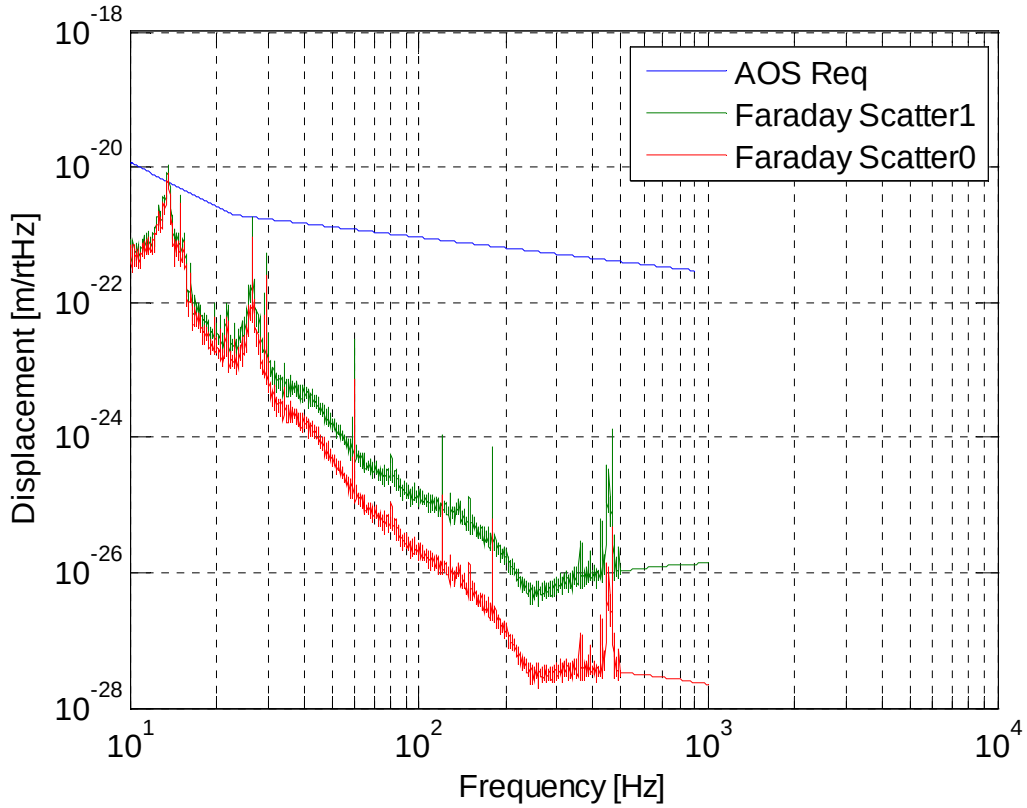

Figure 11: Output Faraday Isolator Scattered Light Displacement Noise

2.5.4 Vertical Blade Spring Design

The Faraday Isolator blade spring suspension does not need to be flat in the loaded condition, because there is no height restriction in the HAM chamber location and there is no requirement to minimize the longitudinal to vertical motion coupling of the Faraday Isolator. A flat blade spring is simpler to design and less expensive to manufacture than a pre-stressed, curved blade spring, as is used for the OMC suspension.

Design equations were developed for the blade springs to suspend the Faraday Isolator optical table, and to suspend the eddy current damping plate. The load is different, and the desired vertical bounce frequency is different for each set of springs. Before committing to fabricate the maraging steel blade springs that will be used for the ADLIGO suspension, a test was made of similar sized springs made out of 1095 spring steel, which is inexpensive, readily available, and does not require heat treating. Blade Spring Tests were performed for the upper and lower Output Faraday Isolator configurations. The test mass required to deflect the blade to the design height agreed with the design value < 10%. The radius of curvature of the loaded blade spring agreed with the design value <1%.The predicted vertical bounce frequency under load agreed with the measured value to 1 %. The results of the tests give confidence that the design equations are accurate to better than 10%.

The design equations are described in T0900324-v1.

2.5.5 Picomotor Pitch Adjustment

We are planning on using the non-sealed UHV model, and specify the better Barrierta IS lubricant. This lubricant is in the LIGO queue for high vacuum compatibility testing.

2.6 Arm Cavity Baffle and COC Wide Angle Baffle

A Viton o-ring suspension will be used to suspend all the baffles and beam dumps that connect to the ISI "0" Ring and from the optical table of the BSC. This includes the Arm Cavity Baffle, Wide Angle Baffle, ITM Elliptical Baffle, FM Elliptical Baffle, and FM Beam Dump.

A prototype of the elliptical baffle suspension was made of a tube 60" long, 2" outer diameter, and 1/16" thick wall that connected the payload to the Viton-damped suspension point, as shown in Figure 12.

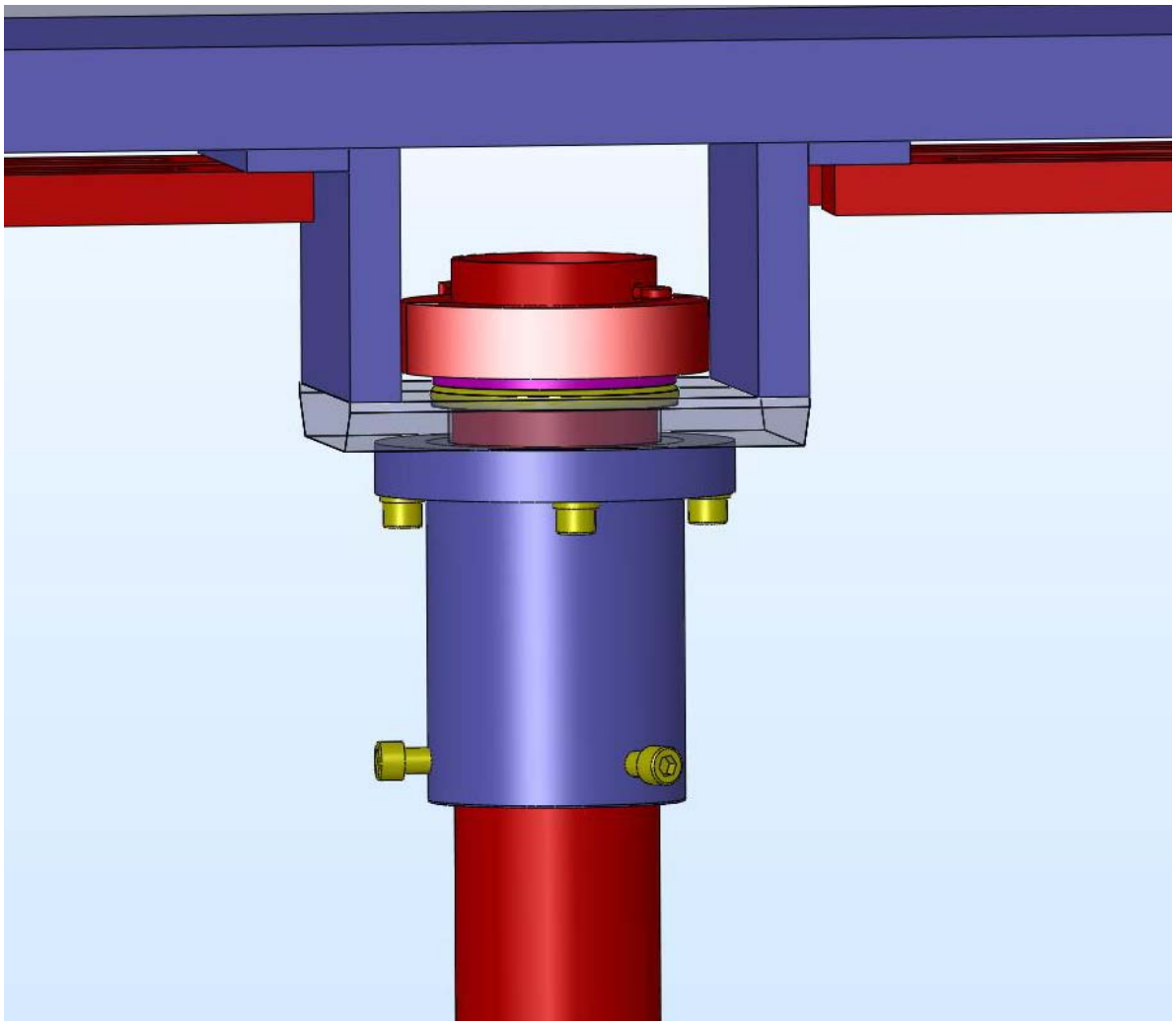

Figure 12: Viton Damped Suspension

The payload of ~50kg was rigidly attached to one end of the tube. A horizontal viton o-ring between the suspension mounting platform and the other end of the tube provided the necessary

mechanical compliances for the payload to oscillate. A more traditional attachment made with a short thick wire between the tube and the platform was also studied for comparison.

2.6.1 Earthquake Stops

The mounting bracket for the Viton-damped suspension provides a collar beneath the support plate that limits the motion of the suspension tube in the event of an earthquake.

2.6.2 Viton O-ring Suspension Data

Figure 13 shows the measured transmissibility of the two elliptical baffle suspensions prototypes for the horizontal direction. The green curve is the o-ring type suspension transfer function and the blue curve is the short wire type suspension. The o-ring suspension provides damping for both the pendulum mode and also the internal modes of the steel tube connecting the payload to the suspension point.

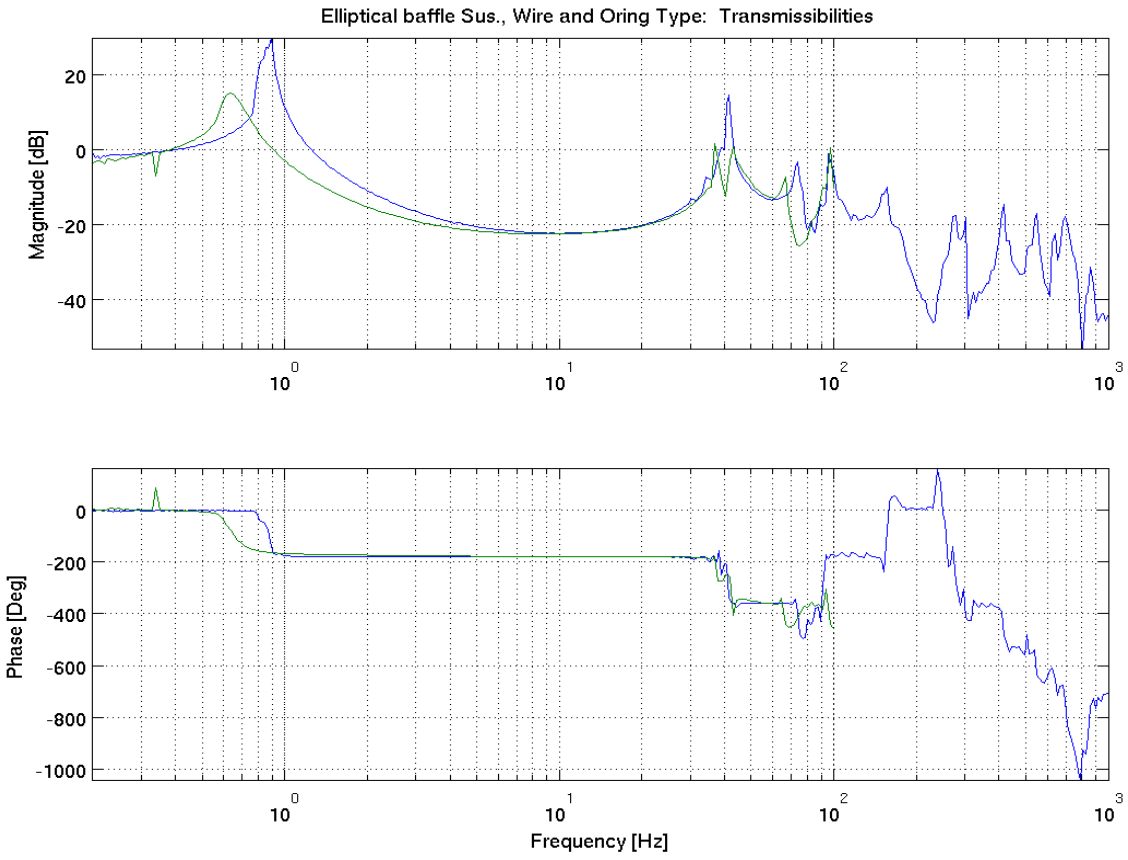

Figure 13: Horizontal transmissibilities of the elliptical baffle suspensions for the o-ring type (green) and the short thick wire (blue).

Figure 14 shows the vertical transmissibility with a stack of 8 viton o-rings measured using the impulse response technique. Only this measurement method could be used because the set-up did not allow vertical excitation of the suspension. This technique works reasonably well at high frequency, but has the difficulty of exciting the low frequency band below ~5Hz. The measurement shows some amount of vertical attenuation above 70 Hz. The vertical fundamental mode has a quite poor quality factor and therefore the resonance is difficult to determine from this type of measurement; it is probability between 10 Hz to 30Hz

Internal modes of the suspension tube can affect the performance of the ISI control loops. To minimize the recoiling effect of these modes against the ISI platform one could use visco-elastic materials around the suspension tube itself to lower the quality factor of the lowest modes.

In addition, the tube internal modes can be moved to a higher frequency by reducing the tube mass and reducing the wall thickness from 1.6 mm to 1mm, by changing the length-diameter ratio, and by adding light stiffeners along the tube. However, it may be difficult to move those resonances above 100 Hz.

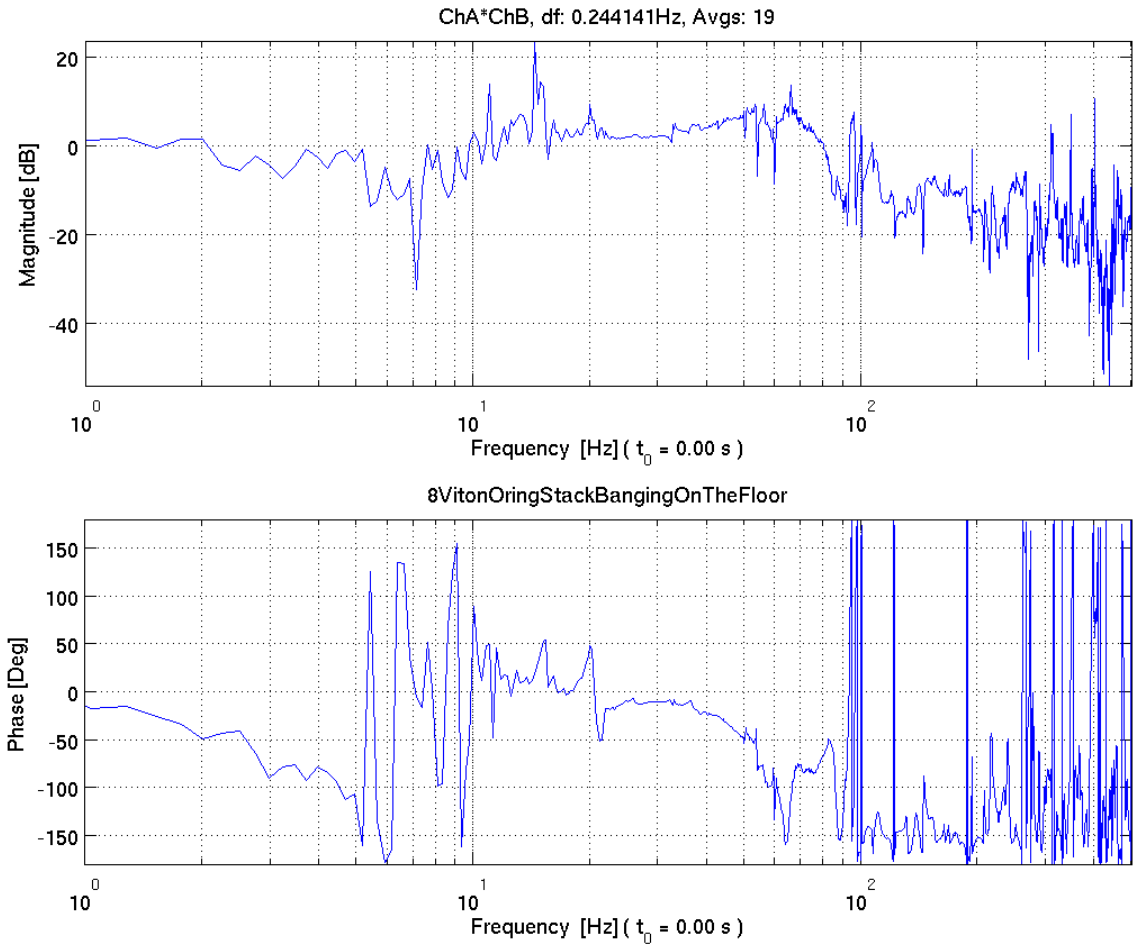

Figure 14: Vertical transfer function of the elliptical baffle suspension with a stack of 8 viton o-rings.

2.6.3 Cylindrical vs Round COC Wide Angle Baffle

2.6.3.1 Round arm cavity baffle vs square?

A cylindrical Wide Angle Baffle is shown behind the louver Arm Cavity Baffle and in front of the ITM HR side of H2 in BSC7 in Figure 15.

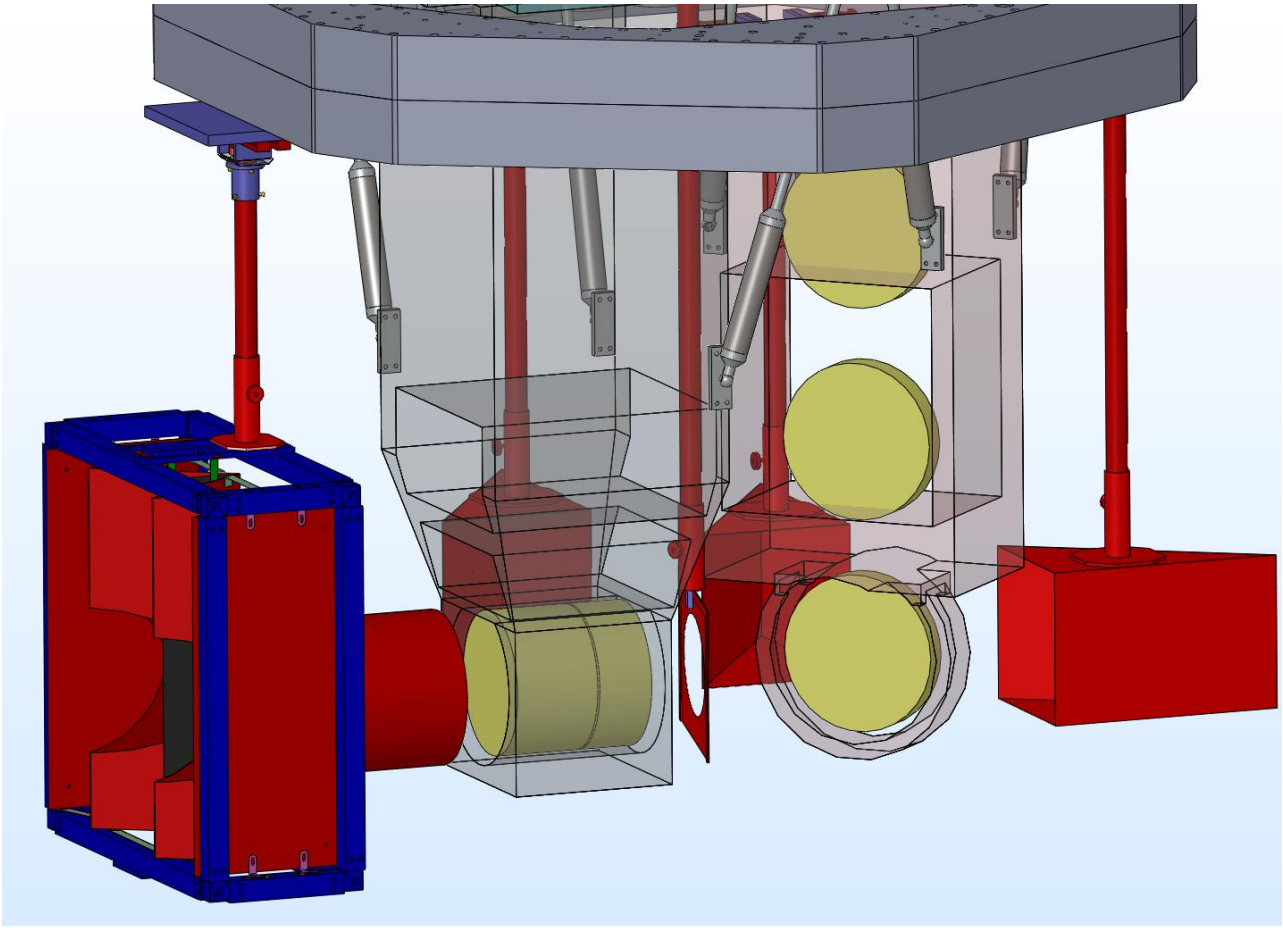

Figure 15: Cylindrical Wide Angle Baffle, H1 ITMX

Similarly in Figure 16, a cylindrical Wide Angle Baffle is shown in front of the ITM HR side of H1 in BSC3.

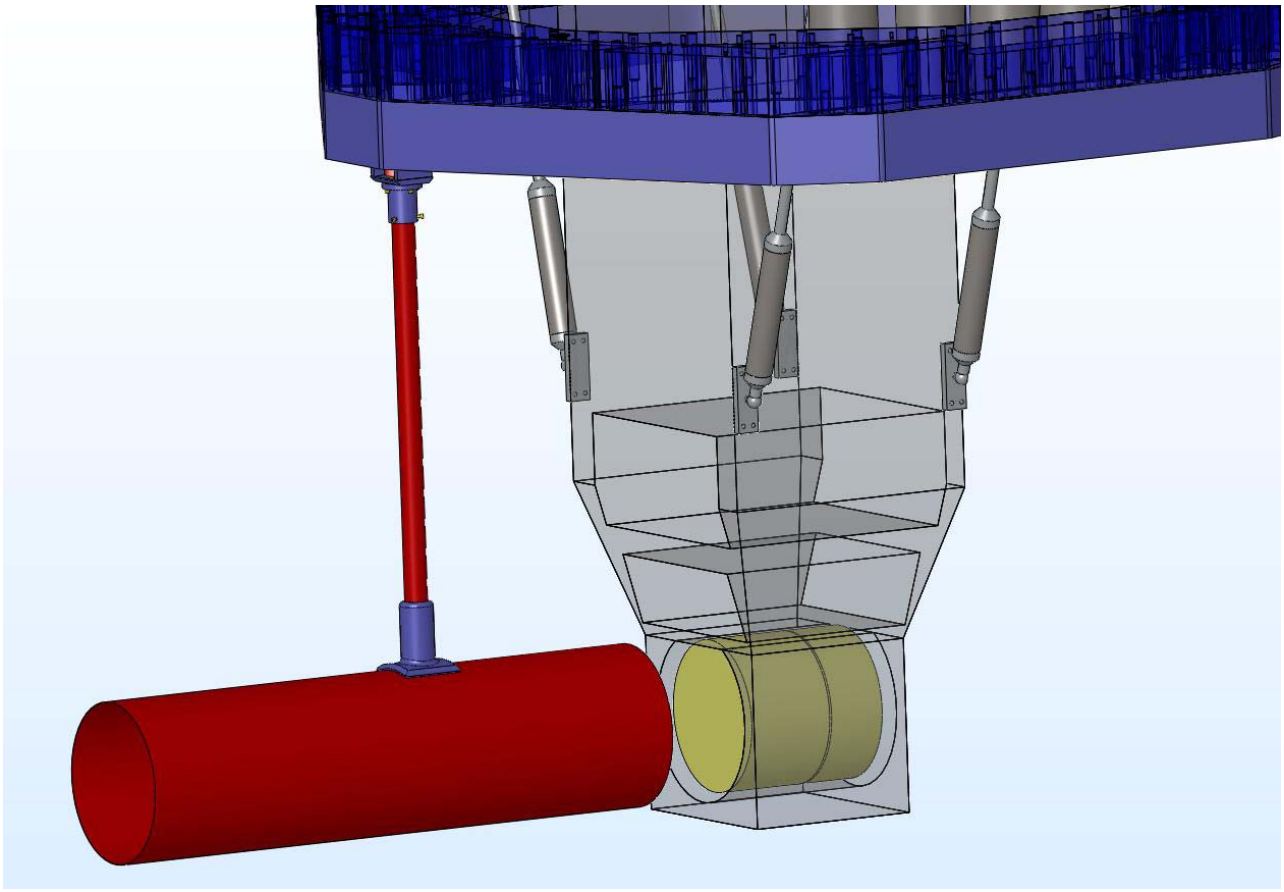

Figure 16: Wide Angle Baffle, H1 ITM on BSC3

2.6.3.2 Access to TM?

2.6.3.3 What happens to light passing between arm cavity baffle ID and OD of TM?

The light scattered down the beam tube that is not caught by the arm cavity baffle will spill over the edge of the ITM mirror and hit the SUS frame. The frame will be assumed to provide a partial glint, represented by a BRDF = 100.

scattered power in annulus between ITM
and the arm cavity baffle, W

$$P_{ann} := P_a \cdot \int_{\theta_{itm}}^{\theta_{ac}} 2 \cdot \pi \cdot \theta \cdot BRDF_1(\theta)\, d\theta$$

$$P_{ann} = 0.0968$$

Power scattered from the ITM SUS into the IFO is

$$P_{anns} := \sqrt{16} \cdot P_{ann} \cdot BRDF_{sus} \cdot \frac{\pi \cdot w_{ifo}^2}{L^2} \cdot BRDF_1(\theta_{coc}) \cdot \Lambda_{ifo}$$

$$P_{anns} = 3.7313\times 10^{-15}$$

displacement noise @ 20 Hz, m/rtHz $\quad DN_{ann} := TF_{itmhr}\cdot\left(\frac{P_{anns}}{P_{psl}}\right)^{0.5}\cdot x_{bsc}\cdot 2\cdot k$

$$DN_{ann} = 3.549\times 10^{-24}$$

This scattered power is below the AOS requirement.

2.6.3.4 Wide angle camera view from a viewport?

The HR surfaces of the ITM in H1 and H2 can be viewed at a wide angle from the viewports in the BSC chamber, as shown in Figure 17. To enable this, the H1 cylindrical baffle is placed 210 mm from the ITM HR surface, and the H2 cylindrical baffle is placed 130 mm from the ITM HR surfaces.

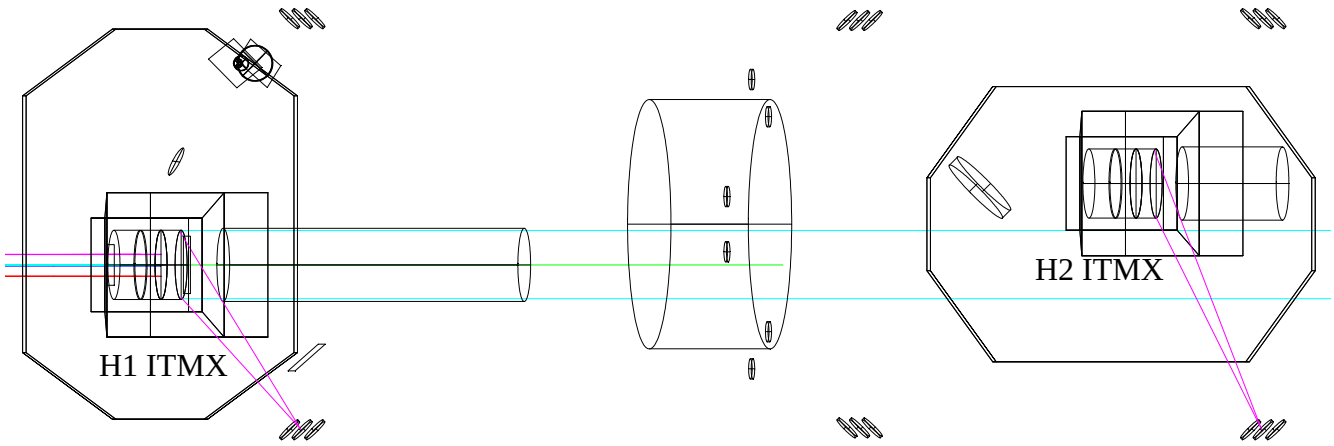

Figure 17: ZEMAX Layout of H1 and H2 ITM Wide Angle Scatter Baffles, With Camera View of the HR Surfaces

The wide angle scattered displacement noise from the BSC, increases with the gap between the ITM HR and the cylindrical baffle, as shown in Figure 18. At the widest gap of 210 mm, the wide angle scattered light from the BSC chamber is still below the AOS requirement, as seen in Figure 22

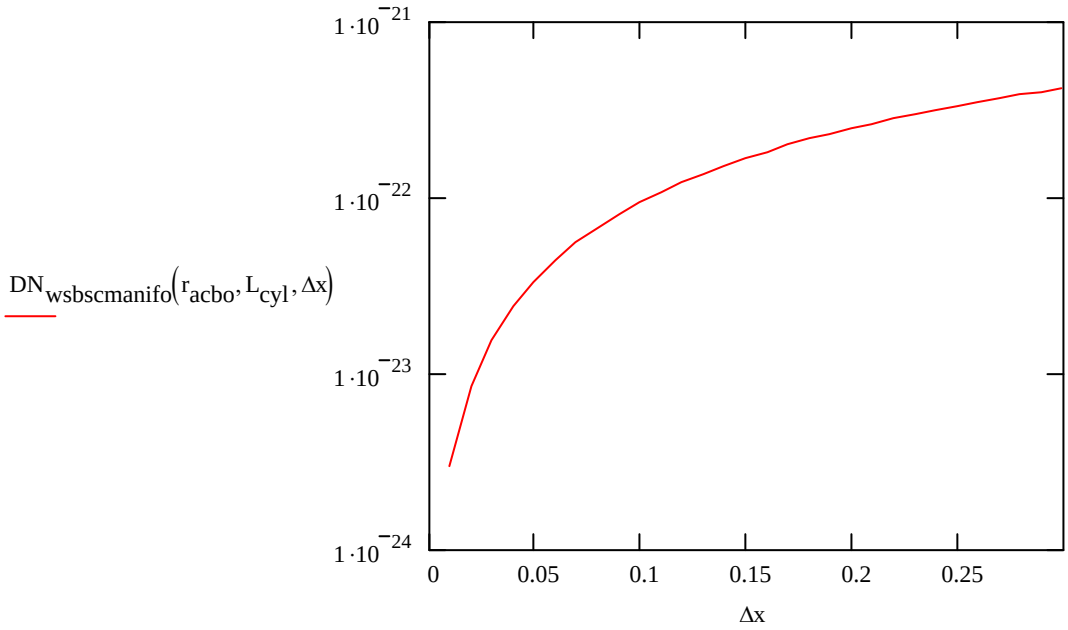

Figure 18: Wide Angle Scattered Displacement noise by the BSC chamber, m/rt Hz @ 10 Hz freq.

2.7 Manifold/Cryopump Baffle

2.7.1 Suspension Design

The combined Manifold/Cryopump Baffle assembly is suspended by wires from two blade springs that mount to the insides of the compression ring, which fastens to the inside of the manifold similar to the design used in ELIGO, as shown in Figure 19. The radius of the blade springs under load matches the inside radius of the compression ring. An adjustment mechanism moves the suspension point longitudinally to coincide with the center of gravity of the suspended assembly.

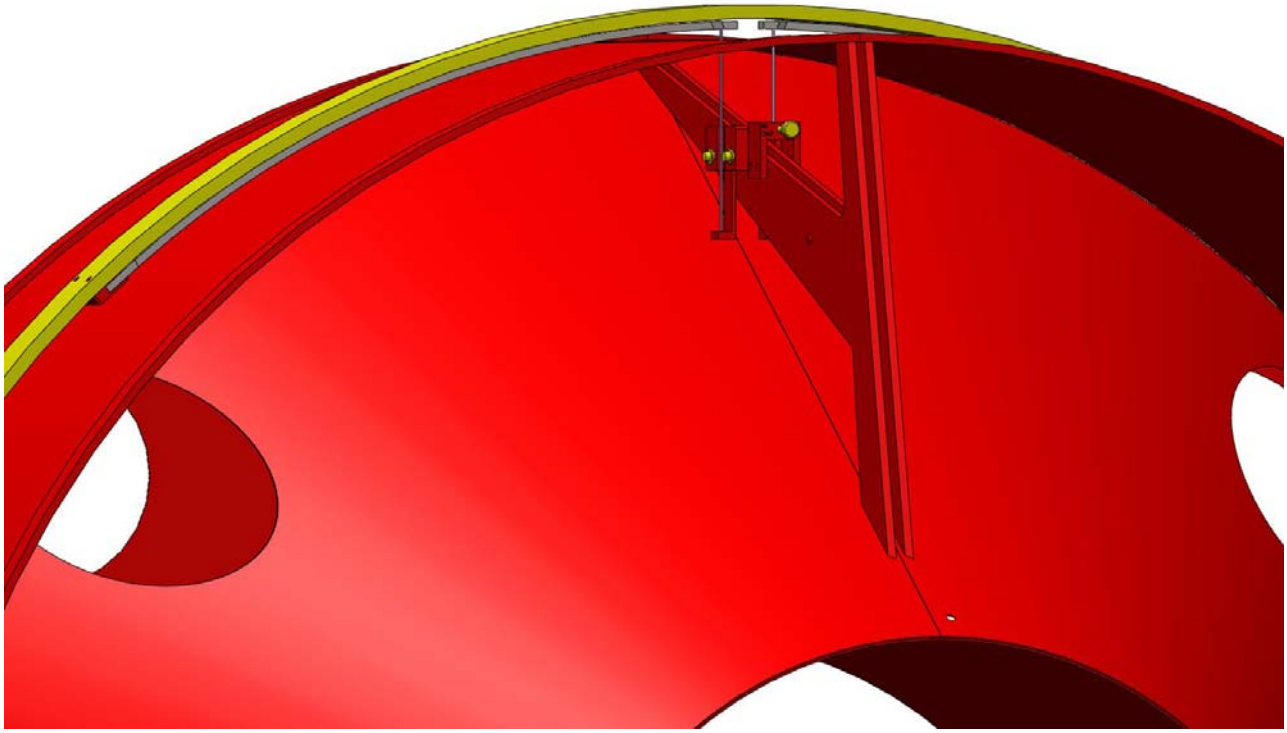

Figure 19: Vertical Blade Suspension Detail, Manifold/Cryopump Baffle

The details of the eddy current damping plate is shown in Figure 20.

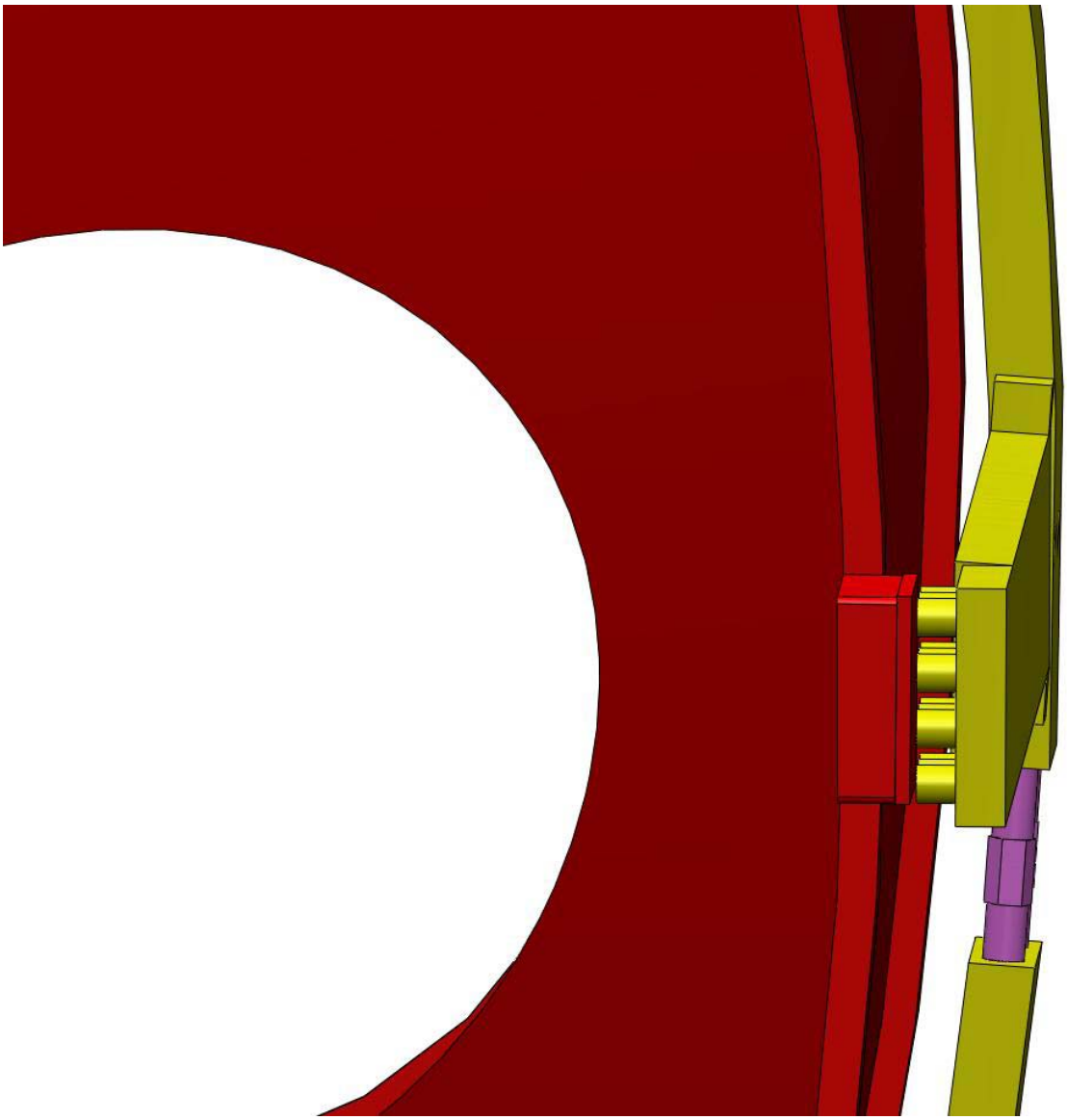

Figure 20: Eddy Current Damping Assembly

The transfer function had a compound pendulum shape as shown in Figure 21.

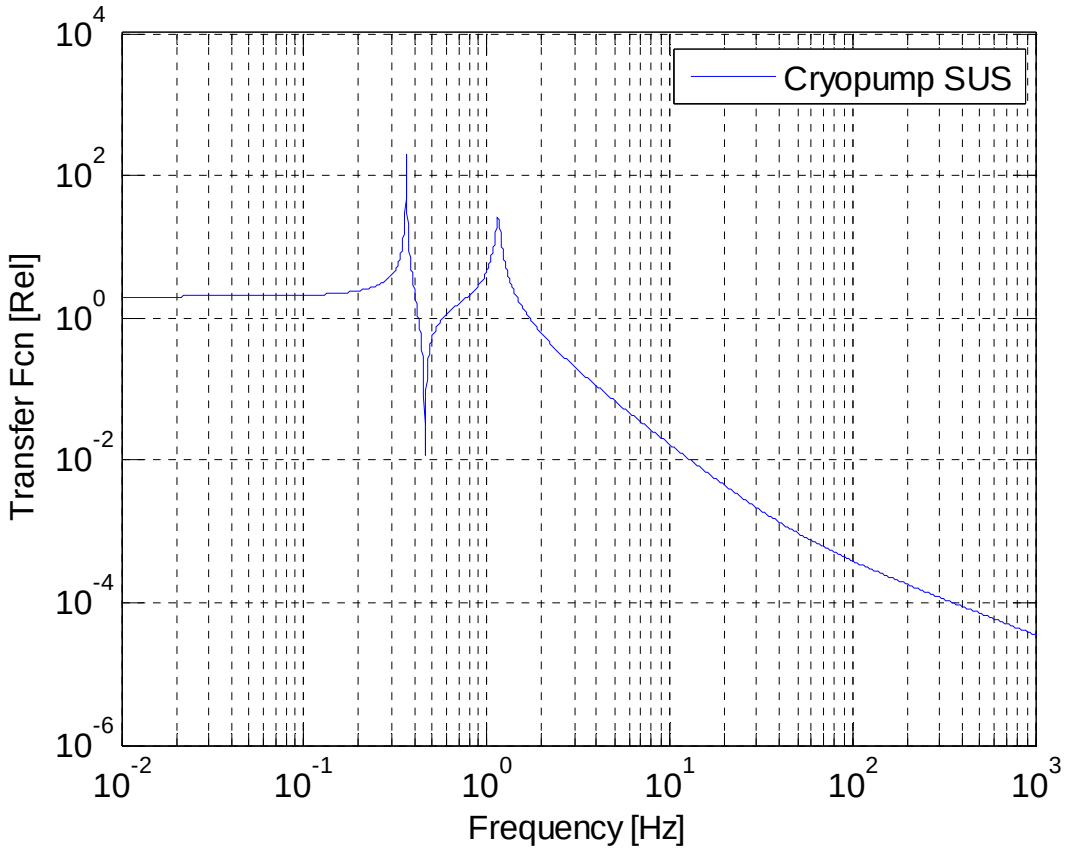

Figure 21: Cryopump Baffle and Manifold Baffle SUS transfer function

2.7.2 Scattering Surfaces

The strengthening struts that are visible inside the manifold baffle cone from the COC direction are angled with sharp corners to eliminate direct reflections back to the COC.

The blank-off flanges and viewports that are visible through the holes in the manifold baffle will scatter light, but will not cause direct reflections of light back to the COC.

2.7.3 Suspension Transfer function

How much margin is available for less than ideal transfer function? The Cryopump Baffle scatter has many orders of magnitude margin.

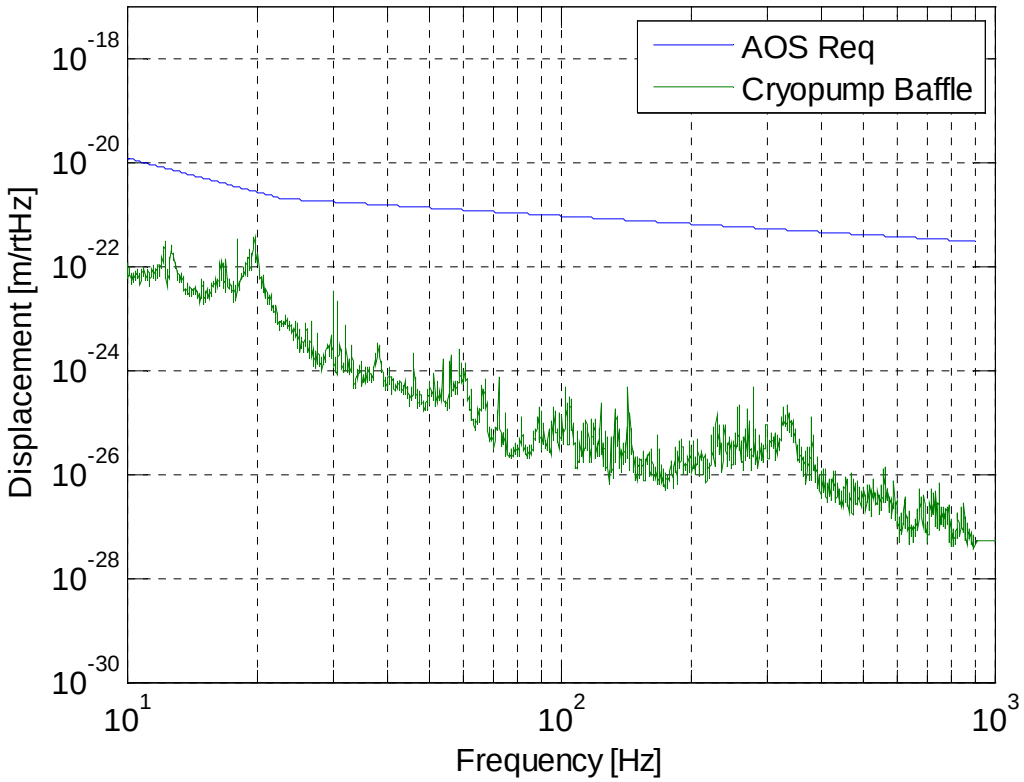

2.7.4 Displacement Noise from Manifold Baffle

The surfaces of the ITM and ETM scatter wide-angle light into four paths: 1) most of that scattered light is captured by the wide-angle baffle that hangs directly in front of the HR surface of the COC; 2) some of the light is scattered at angles close to 90 deg from the normal to the COC surface and will hit the walls of the BSC chamber and re-scatter from the COC into the IFO mode; 3) some of the light will pass through the holes in the arm cavity baffle and will hit the manifold wall and re-scatter from the COC into the IFO mode; and 4) some will hit the suspended manifold baffle and re-scatter—the manifold baffle hides the corner of the manifold/viewport flange and avoids the retro-reflection.

The scattered light displacement noise from sources 2, 3, and 4 is shown in Figure 22.

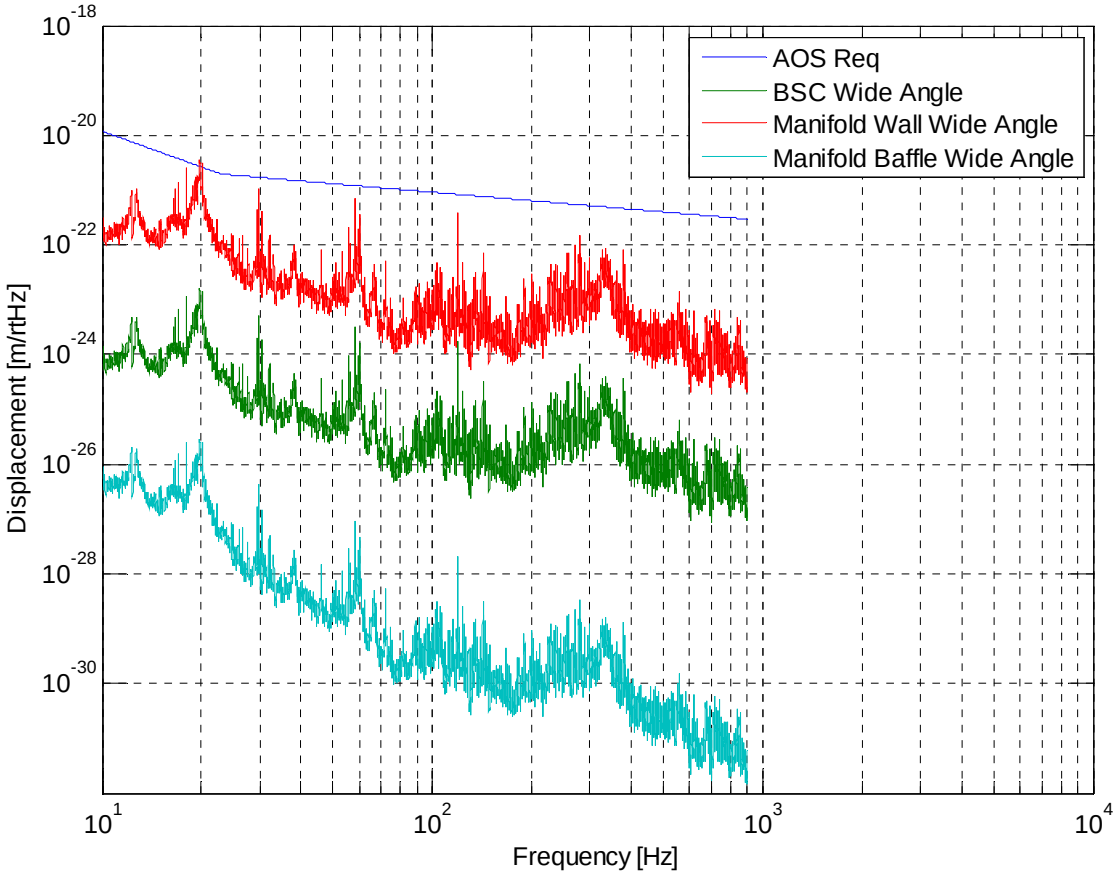

Figure 22: COC Wide Angle Scattered light from 1) BSC chamber, 2) Manifold Wall, and 3) Manifold Baffle

2.7.5 Edge Diffraction from the edges of the Cryopump Baffle?

2.8 Elliptical Baffles and H2 beam dumps

2.8.1 PRM Elliptical Baffle

Hiro Yamamoto determined with FFT modeling that the optimum signal to noise occurs when the recombined beams in the recycling cavity at the BS have an approximately elliptical beam cross-section with 224 mm horizontal diameter and 259 mm vertical diameter (see G070657 LSC-Virgo Meeting).

The ITM and PRM Elliptical Baffle clear apertures were chosen to match those dimensions.

A further function of the PRM Elliptical baffle is to keep the oversize Gaussian beam in the power recycling cavity beam from hitting the structure of the BS suspension, as shown in Figure 23.

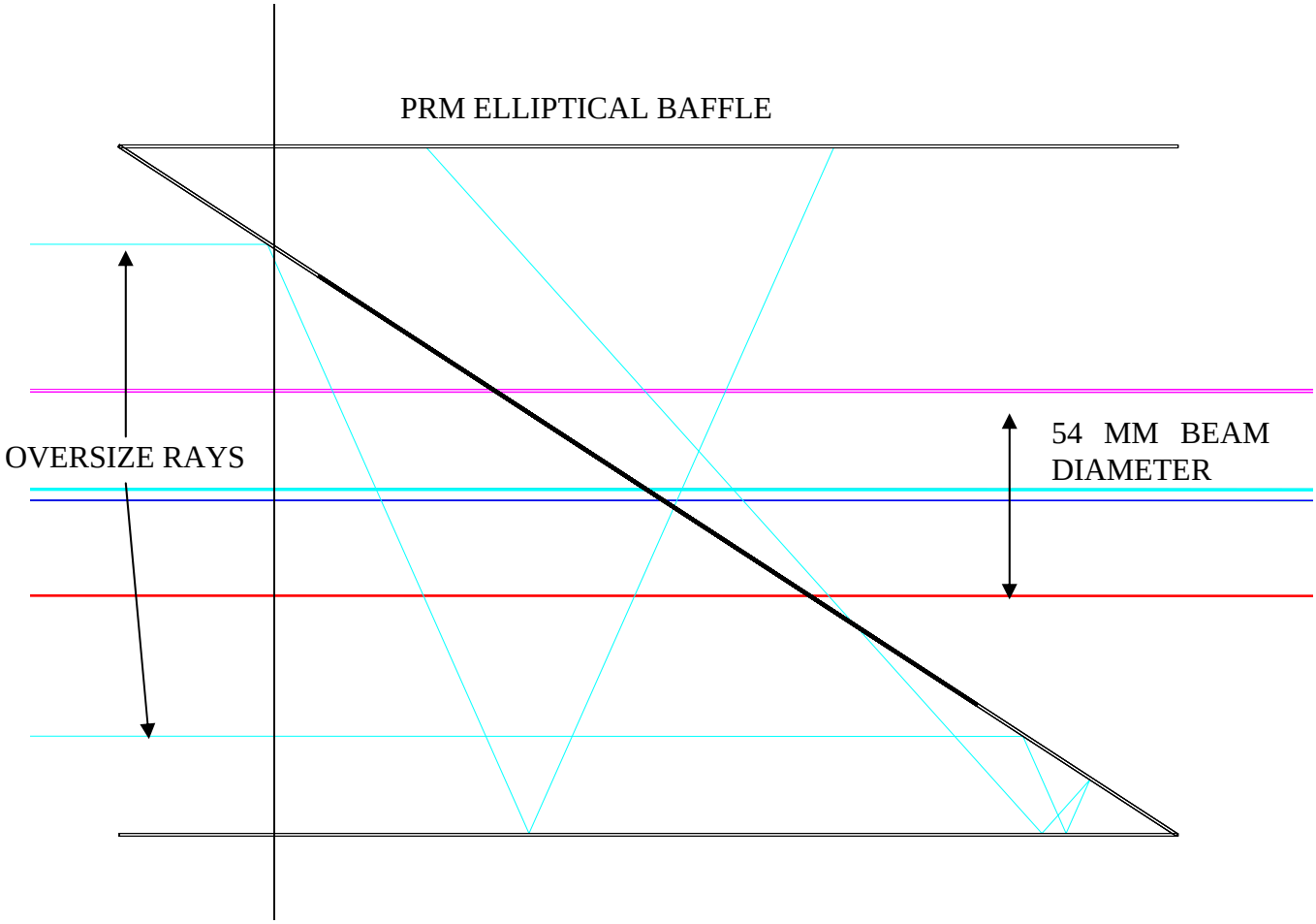

Figure 23: PRM ELLIPTICAL BAFFLE

Likewise, the ITM Elliptical baffles serve the same function in keeping the oversize Gaussian beams from the arm cavity from hitting the structure of the BS suspension.

Additionally, the ITM Elliptical baffles function as beam dumps to catch the ITM and CP ghost beams, as shown in Figure 24.

The scattered light displacement noise that would occur, if the PRM Elliptical baffle were not present and the Gaussian beam from the PR3 would hit the suspension structure of the BS and eventually scatter from the chamber walls, is shown in Figure 25. The noise is four orders of magnitude lower than the requirement; therefore, the PRM Elliptical Baffle will be eliminated.

2.8.2 ITM Elliptical Baffle

The ITM Elliptical baffles serve the same function in keeping the oversize Gaussian beams from the arm cavity from hitting the structure of the BS suspension.

Additionally, the ITM Elliptical baffles function as beam dumps to catch the ITM and CP ghost beams, as shown in Figure 24.

The scattered light displacement noise that would occur, if the ITM Elliptical baffle were not present and the Gaussian beam from the arm cavity would hit the suspension structure of the BS

and eventually scatter from the chamber walls, is shown in Figure 25. Therefore, the ITM Elliptical baffle is needed to control the scattered light.

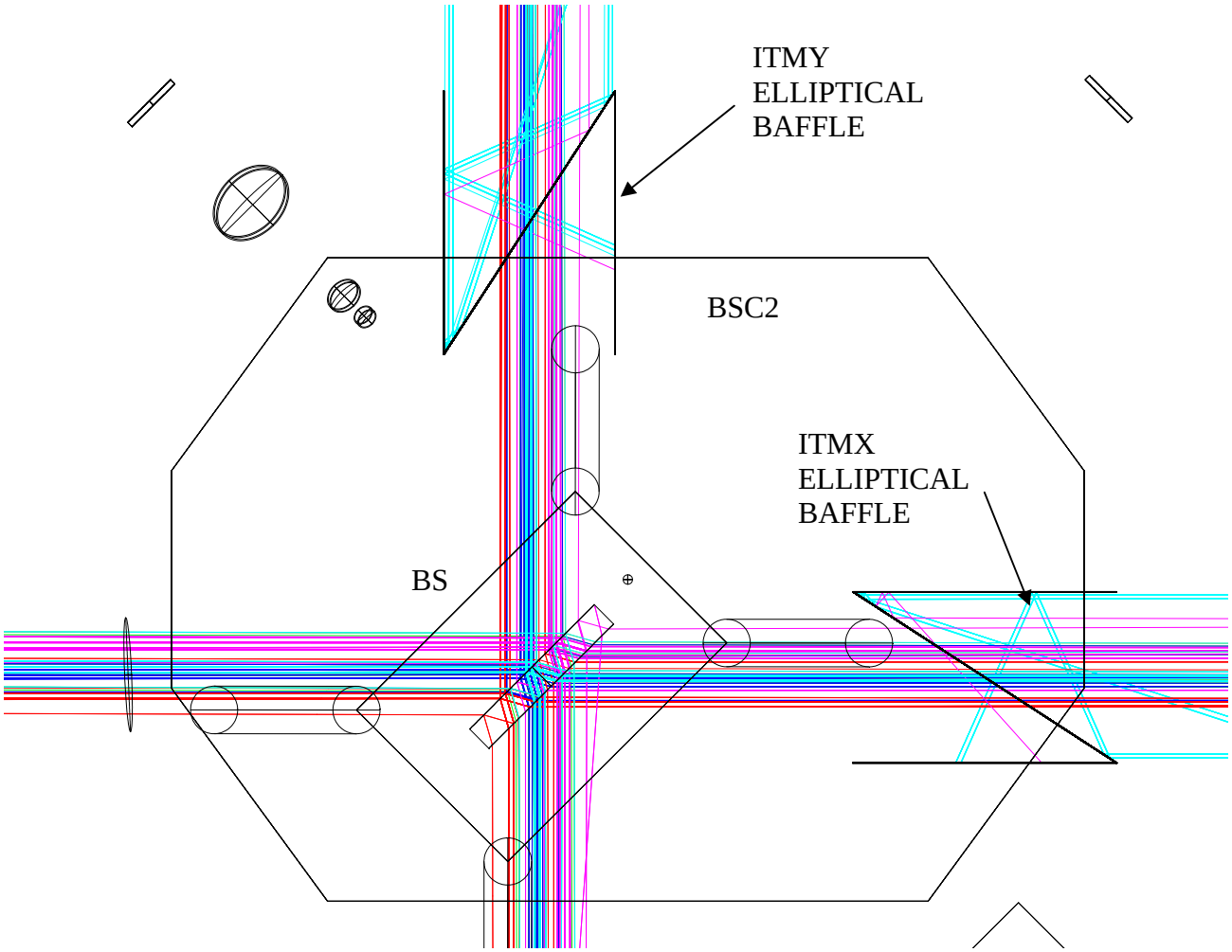

Figure 24: ITM Elliptical Baffle

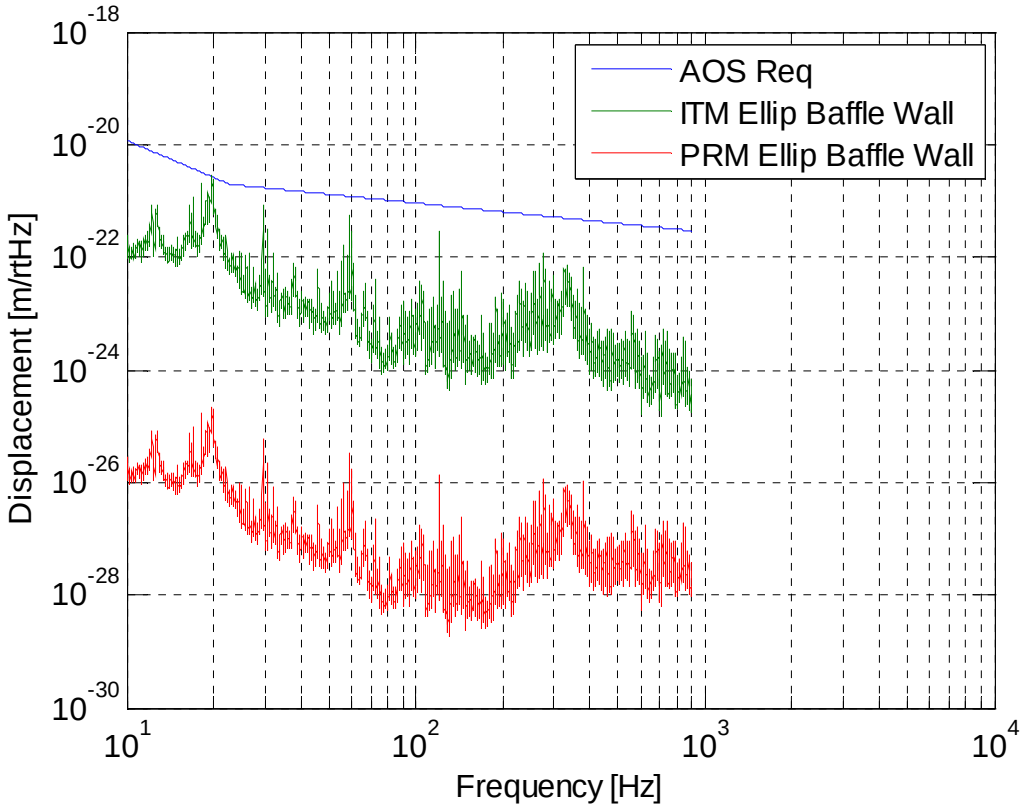

Figure 25: Displacement Noise without the PRM and ITM Elliptical Baffle

2.8.3 H2 Elliptical Scraper Mirror

2.8.4 H2 Scraper Beam Dump

Why needed? Aperture determined by Hiro's Calculations: show reference.

There is a beam dump on the ITM side of the scraper mirror to catch the "scraped" excess power from the arm. The PRM elliptical baffle on HAM9 shapes the beam to the size of the scraper mirror, so no power hits the scraper mirror from the power recycling side.

2.8.5 H2 Fold Mirror Beam Dump

2.8.6 Scattering from Walls without H2 scraper mirror and beam dump

Do we need these dumps, or the beam dumps be plates attached to the walls?

2.9 Miscellaneous

2.9.1 If black glass is used will it crack?

Black glass will be used for the plate beam dumps, SRM, SR2, SR3. The power is relatively low in the signal recycling cavity and these ghost beams will not cause excessive heating to the black glass.

2.9.2 Is there a hazard due to handling baffles with sharp edges?

Yes. Most of the baffles are made from 0.047 in thick stainless steel that have been laser cut. The edges are purposefully sharp, and must be handled with care to avoid cutting the skin and/or the rubber gloves during installation. The Hazard Analysis will address this issue.

2.9.3 Scattering from wide angle COC to nearby suspension structure?

The wide angle scattering from the ITM and ETM that misses the Wide Angle Baffle was assumed to hit the chamber walls and re-scatter into the IFO mode. This is a worse case than scattering from the nearby suspension. It is not likely that the wide angle scattered rays would make a glint reflection back toward the COC.

The calculated wide-angle scatter displacement noise from the BSC chamber is shown in Figure 22.

2.10 H1-H2 Mid-station Baffle Design

2.10.1 H1-H2 Cross-talk Ray Geometry

A Mid-station Baffle will be placed at the midpoint of the H1 and H2 interferometers to block the small angle scattered light from the test mass (TM) of H1 coupling into the opposite TM of H2. The baffle will block the line of sight between the H1 and H2 test masses, as shown in Figure 26. The closest separation of the baffle edge from the IFO beam center is 30 mm. The beam waist size at the mid-station is 11.5 mm radius.

The mid-station baffle can be either a vertical plate, 340 mm wide by approximately 1000 mm tall, or a 1000 mm diameter baffle with two horizontal holes of 30 mm diameter to allow passage of the H1 and H2 beams.

The baffle will be suspended by wires from blade springs attached to a compression ring mounted against the manifold inner wall at the VEA in the mid-station, similar to the manifold/cryopump baffle suspension, and damped with eddy current magnets attached to the manifold wall. The calculation was made for a vertical baffle; however, the baffle will be tilted forward to minimize the scattering and the direct reflection down the beam tube, and to provide more surface area for radiation cooling.

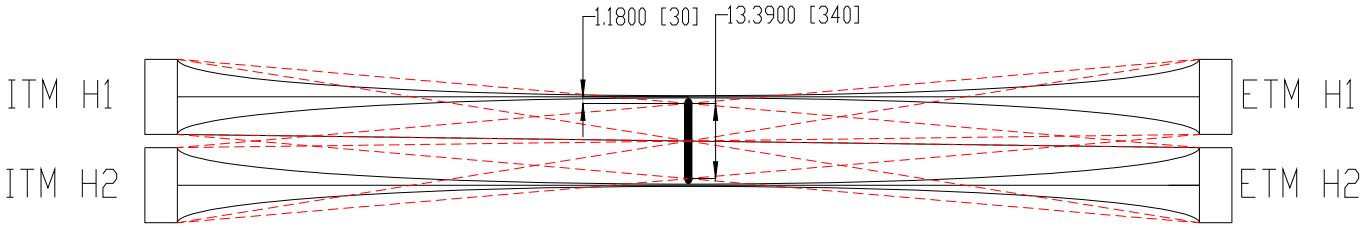

Figure 26: Ray paths from H1 and H2 blocked by the Mid-station Baffle

Without the baffle in place, we estimate that the cross-coupled power scattered from each opposite test mass, e.g. from ETMH1 to ITMH2, is 1.2W.

2.10.2 Interferometer Power Loss caused by Mid-station Baffle

The power loss fraction from the edge of the vertical baffle intruding into the interferometer main beam is 2.8 E-7 for a separation of 30 mm, as shown in Figure 27.

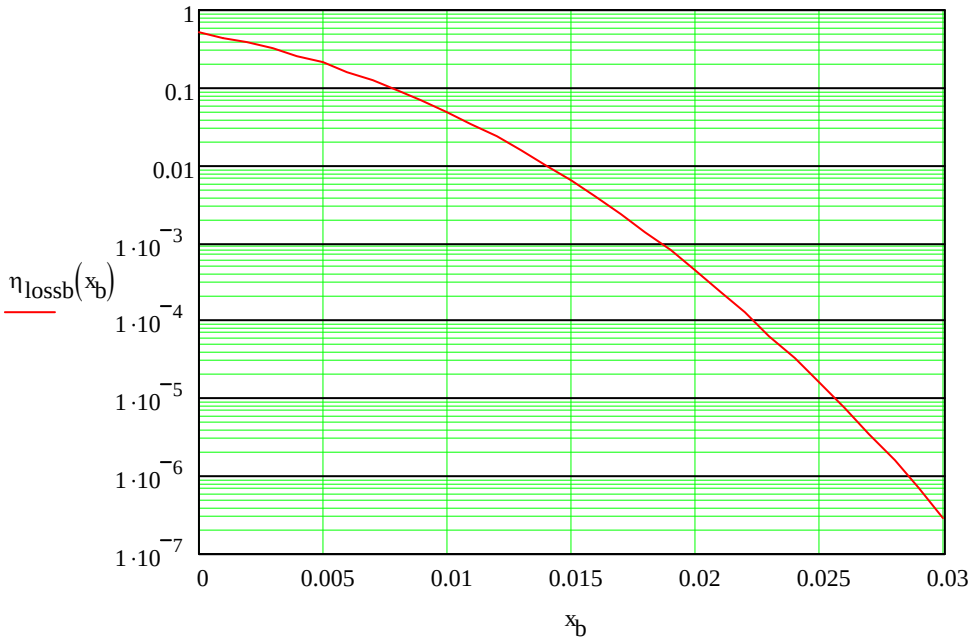

Figure 27: Power loss for mid-station baffle intruding into the interferometer beam

2.10.3 Edge Diffraction from Mid-station Baffle

The power scattered by the opposite test mass down the arm beam tube to the mid-station was calculated using the BRDF of the CSIRO, S/N 2 pathfinder optic of Initial LIGO.

$$P_{sms} = 22.3\ W$$

We will model the Mid-station baffle as being a vertical plate with an edge length H_b equal to the diameter of the arm beam tube, 1.06 m.

The power diffracted by the baffle edge is the fraction of the total power uncovered by the moving baffle as it displaces laterally a distance x due to its seismic motion[1].

Motion of beam tube @ 20 Hz, m/rt Hz $x_{beamtube} := 10^{-9}$

lateral motion of baffle, m $x := x_{beamtube}$

area uncovered by moving edge, m^2 $A_{edge} := H_b \cdot x$

total area of mid-station, m^2 $A_{ms} := \pi \frac{H_b^{\,2}}{4}$

power diffracted from edge $P_{de} := \frac{4 \cdot x}{\pi H_b} \cdot P_{sms}$ $P_{de} = 5.360 \times 10^{-10}$

The coherence length along the diffracting edge is approximately the diameter of the interferometer beam waist. This piece of the vertical edge will diffract light as a cylindrical wave with a fixed height $2*w_{ifo}$ and a radius = Lmb. The power from each coherence length along the length of the edge will add in quadrature.

IFO waist size, m $w_{ifo} := 0.0115$

IFO mid-station length, m $L_{mb} := 2000$

number of coherence lengths within the baffle edge $N := \frac{H_b}{2 \cdot w_{ifo}}$ $N = 46.087$

The fraction of this light that intercepts the interferometer mode area on the far test mass is given by the ratio of the solid angle subtended by the mode area at the location of the test mass to the solid angle of the cylindrical wave.

solid angle subtended by diffracted cylindrical wave, sr^-1 $\Omega_{cyl} := \frac{2 \cdot \pi \cdot L_{mb} \cdot 2 \cdot w_{ifo}}{L_{mb}^{\,2}}$

solid angle subtended by IFO mode area at COC, sr^-1 $\Omega_{COC} := \frac{\pi \cdot w_{ifo}^{\,2}}{L_{mb}^{\,2}}$

[1] Private communication, Kip Thorne

fractional solid angle subtended by the COC $\eta := \frac{w_{ifo}}{4 \cdot L_{mb}}$ $\eta = 1.438 \times 10^{-6}$

The light that hits the test mass will scatter into the solid angle of the interferometer mode.

edge diffracted power scattered into IFO $P_{des} := \sqrt{N} \cdot P_{de} \cdot \eta \cdot BRDF\left(30 \cdot 10^{-6}\right) \cdot \Delta_{ifo}$

$P_{des} = 1.941 \times 10^{-20}$

When the baffle edge moves and uncovers the diffracted power, the length of the ray path from the baffle edge to the test mass increases longitudinally and causes a phase shift of the diffracted field entering the interferometer.

angle subtended by displaced edge from center of COC $\theta_{diff} := \frac{x_b}{L_{mb}}$

longitudinal displacement of source, m $y_\phi := x_{beamtube} \cdot \theta_{diff}$

Transfer function @ 20 Hz, ITM HR $TF_{itmhr} := 1.1 \cdot 10^{-9}$

displacement noise @ 20 Hz, m/rtHz $DN_{mbed} := TF_{itmhr} \cdot \left(\frac{P_{des}}{P_{psl}}\right)^{0.5} \cdot y_\phi \cdot k$

$DN_{mbed} = 2.862 \times 10^{-34}$

The edge-diffracted displacement noise of the Mid-station Baffle is shown in Figure 28.

2.10.4 Scatter from Mid-station Baffle

The small-angle scattered power from the H1 and H2 ETM and ITM hits the mid-station baffle and will scatter back to the mode waist area at the COC source and re-scatter from the COC into the interferometer mode. The 8 scattering surfaces, 4 sources per arm times 2 arms, are incoherent and will add in quadrature.

The power scattered from each test mass to the mid-station baffle is

$P_{sb1} = 8.057$

power scattered by mid-station baffle, W $P_{mbs} := \sqrt{N_{mbs}} \cdot P_{sb1} \cdot BRDF_{mb} \cdot \frac{\pi \cdot w_{ifo}^2}{\left(\frac{L}{2}\right)^2} \cdot BRDF\left(30 \cdot 10^{-6}\right) \cdot \Delta_{ifo}$

$P_{mbs} = 4.392 \times 10^{-16}$

The baffle suspension motion transfer function is similar to the manifold/cryopump baffle TF damped suspension.

attenuation of mid-station baffle suspension @ 100 Hz

$$mbatten := 2 \cdot 10^{-3}$$

displacement noise @ 100 Hz, m/rtHz

$$DN_{mbs} := TF_{itmhr} \cdot \left(\frac{P_{mbs}}{P_{psl}} \right)^{0.5} \cdot x_{beamtube} \cdot 2 \cdot k \cdot mbatten$$

$$DN_{mbs} = 9.741 \times 10^{-25}$$

The scattered light displacement noise of the Mid-station Baffle is shown in Figure 28.

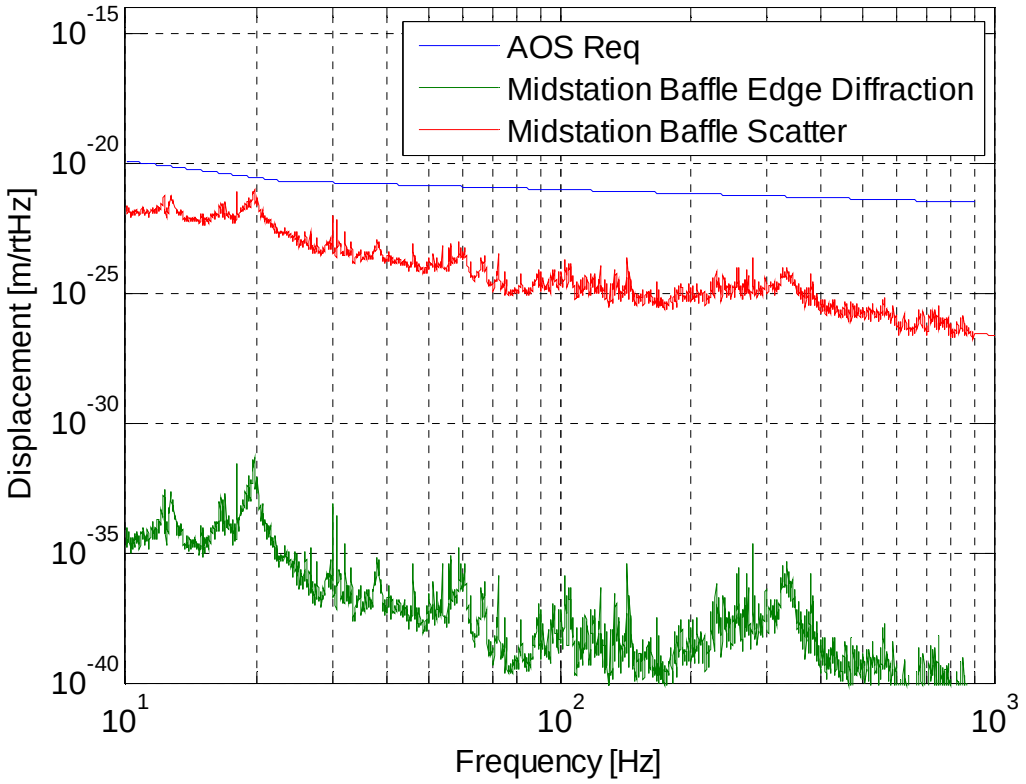

Figure 28: Scatter and Edge Diffraction Displacement Noise from the Mid-station Baffle

2.10.5 Heating of Mid-station Baffle

The power scattered from the 4 H1 and H2 test masses at opposite ends of the arm beam tube will be absorbed by the mid-station baffle and increase its temperature. Radiation cooling will suffice to remove the heat.

power scattered from 4 COC to mid-station baffle, W

$$P_{sball} := 4 \cdot P_{sb1}$$

$$P_{sball} = 32.229$$

Stephan-Boltzmann constant, W/m^2/K^4

$$\sigma := 5.67 \cdot 10^{-8}$$

area of baffle, m^2

$$A_b := H_b \cdot W_b(x_b)$$

geometrical factor

$$F := 1$$

wall temperature, deg K

$$T_w := 20 + 272$$

equilibrium temperature of baffle, deg K

$$T_b := \left(\frac{P_{sball}}{\sigma \cdot A_b \cdot F} + T_w^{4} \right)^{\frac{1}{4}}$$

$$T_b = 306.690$$

temperature rise of baffle, deg C

$$\Delta T_b := T_b - T_w$$

$$\Delta T_b = 14.690$$